A Study of Corrosion on Electrodeposited Superhydrophobic Copper Surfaces

S.M.A Mousavi, R. Pitchumani[1]

Advanced Materials and Technologies Laboratory

Department of Mechanical Engineering

Virginia Tech

Blacksburg, Virginia, VA 24061-0238

ABSTRACT

This study considers the corrosion characteristics of superhydrophobic copper surfaces with multiscale asperities formed inherently on a copper substrate, fabricated using a facile, low energy, electrodepostion method. A systematic study is presented for the first time on the effect of surface functionalization time for long-term immersion in a wide range of corrosive environments from the extremely acidic to the extremely alkaline. The corrosion resistance is also reported for the first time as a function of temperature in the range 23–85°C. The superhydrophobic surfaces are shown to enhance corrosion resistance by up to four orders of magnitude compared to bare copper.

KEYWORDS: superhydrophobicity; electrodeposition; copper; corrosion; salt solution; acidic and basic solution.

1. INTRODUCTION

With the rapid growth of industrialization, corrosion is an omnipresent problem that imposes economic and environmental costs all over the world. While corrosion cannot be eliminated, various methods such as cathodic protection, anodic passivation, electrolyte inhibition or the combination have been pursued in order to slow down the corrosion kinetics. From a theoretical standpoint, adsorption of corrosive ions and species on a surface can be deterred by minimizing the wetted solid-electrolyte contact area and thereby lowering the corrosion rate. Inhibiting corrosion on copper, as a material of interest for many applications, has drawn attention for decades and there are several methods used in practice. For instance, utilizing heterocyclic

[1] Corresponding Author; pitchu@vt.edu, +1 703 538 3772

compounds (such as azole derivatives) [1], organic inhibitors [2], and conjugated double bonds [3] are among some of the methods, but their toxicity poses serious risks to humans and environmental life. Alternative methods based on coatings, such as electroactive conducting polymer coatings, are susceptible to water permeability, and the use of self-assembled monolayers to prevent copper corrosion generally suffers from poor durability [4].

The presence of an air cushion in the inter-asperity regions of a solid surface can produce a non-wetting characteristic [5, 6] that can mitigate surface corrosion. Nature, throughout years of evolution, has already mastered such effect by creating superhydrophobic surfaces where the water-solid contact area is minimized [7-10] , which has helped them survive the aggressive environment of their habitat. It is, therefore, of interest to explore the corrosion behavior of practical materials with engineered superhydrophobicity. In general, hydrophobicity is attributed to surfaces with a water contact angle above 90 and below 150 degrees, whereas superhydrophobicity is achieved when surfaces exhibit sustained water contact angles above 150 degrees and contact angle hysteresis below 10 degrees. Studies in the literature have identified two surface modifications to be responsible for producing the superhydrophobic effect: the first is the surface roughness, with structures ranging from micro- to nano-scales, and the second is a chemical coating with low surface energy molecules. Generally, chemical groups are ordered in decreasing order of surface energy as CH_2, CH_3, CF_3, CH_2F, CF_3, and even with CF_3 or other low surface energy materials as the coating on a smooth surface, the highest water contact angle reported does not exceed 130 degrees [11, 12]. This suggests that chemical modification alone is insufficient in providing superhydrophobicity in applications. Use of superhydrophobic surfaces, created through a combination of structural and chemical modification via different methods, has been studied in the literature for their corrosion inhibition characteristics. Various methods are used for the creation of roughness, such as templating, sol-gel method [13-15], electrospinning [16], laser etching [17], hydrothermal synthesis [18], anodization [19], plasma techniques [20, 21], and electrodeposition [22-24]. However, not all the approaches are suitable for large-scale fabrication. For example, the hydrothermal method, despite using environmentally friendly chemicals in the process (such as H_2O or dilute H_2O_2) [25], has to be done under high temperatures and pressures, raising the cost and complexity of fabrication. Etching, on the other hand, is a relatively simple process, but one that involves a mixture of harsh etchants (such as HCl, HF, etc.) [26, 27]. Among the fabrication methods, electrodeposition has been widely used

[28] due to its low cost of fabrication, scalability regardless of surface size and shape, simplicity of the fabrication process at atmospheric pressure and room temperature [29-31], and the controllability of the resulting surface morphology [32].

The preparation of the superhydrophobic surface on various metallic and non-metallic surfaces via different methods including different electrodeposition approaches has been an active area of research in recent years. For a broader discussion on different methods and different substrates, the reader is referred to recent reviews [33, 34]. Herein, keeping with the present focus, the literature on fabrication of superhydrophobic copper surfaces using the constant potential electrodeposition method is reviewed. There have been a number of studies on characterizing electrodeposited superhydrophobic coating on a copper surface in a corrosive environment such as seawater. He et al. [29] electrodeposited zinc on copper at –1.35 V overpotential for 25 minutes, followed by 60 minutes of annealing at $190°C$, and reported a superhydrophobic surface. The anticorrosion behavior of the surface was studied in 3.0% NaCl solution at room temperature, and was reported to exhibit a lower corrosion current and more cathodic corrosion potential compared to bare copper sample. Liu et al. [35] fabricated superhydrophobic copper surface via electrodeposition in cerium chloride and myristic acid electrolyte at atmospheric condition after applying 20V DC overpotential for 30 minutes. The prepared surfaces showed anticorrosion behavior compared to bare copper sample in terms of a lower corrosion current and a more noble corrosion potential. The stability of contact angle after 10 hours of immersion in different pH (1-14) solutions was also reported. Liu et al. [36] fabricated multiscale roughness via nucleating copper sulfate on top of a copper substrate by immersion of the substrate in the electrolyte mixture at $60°C$ for 1.5 hours, followed by modification of the samples with 0.5 wt.% stearic acid for 0.5 hours to achieve superhydrophobicity. The corrosion current on the surface was reported to decrease about two orders of magnitude in 3.5 wt.% NaCl solution and the corrosion potential was shown to shift 50 mV toward nobility compared to a bare copper sample. The stability in different pH environment was characterized by contact angle measurements in the range of pH between 2 and 12. The fabricated surfaces were reported to withstand 24 hours of long-term immersion but deteriorate after 48 hours in 3.5 wt.% sodium chloride solution.

Su et al. [31] electrodeposited nickel on a copper substrate at a constant current density of 0.75 $A.cm^{-2}$ at $50°C$ for 1 hour, followed by 2 hours of drying at $80°C$, and surface treatment

with AC-FAC at 110°C for 1 hour. The chemical stability was measured in terms of the contact angle of droplets with different pH ranging from 1 to 13 on the as-fabricated superhydrophobic surface. The corrosion resistance was shown to improve in 3.5% NaCl solution by means of a lower corrosion current density relative to a bare copper sample. Wang et al. [37] electrodeposited copper on steel substrate at 10 V overpotential for 5 hours and reported good stability of the surfaces with regard to CA for 3 days of immersion in 3.5% NaCl solution. Wang et al. [38] used electrochemically grown laurylamine copper complex on copper substrate at 50V for 1 hour to fabricate superhydrophobic surfaces, which lowered corrosion current density in a 3.5% NaCl solution but degraded the contact angle below 150 after 4 days immersion in 3.5% NaCl solution. Liu et al. [39] fabricated superhydrophobic copper samples via electrodeposition at 20 V for 0.5 hour in myristic acid and cerium chloride mixed with ethanol as the electrolyte. The corrosion inhibition test showed about two orders of magnitude decrease of corrosion current compared to bare copper in 3.5% NaCl solution.

From the foregoing discussion, it is evident that the corrosion studies in the literature on electrodeposited non-wetting surfaces with constant potential method are based on fabrication using relatively high voltages, 5 to 20 volts, for a minimum duration of 0.5 h to 5 h. However, a drawback of such methods is that higher overpotentials and longer process durations lead to an increased system and energy cost. Furthermore, a systematic corrosion study of non-wetting surfaces over a range of harsh chemical environments is lacking. Moreover, with regard to stability, there is a shortage of information on corrosion performance in a harsh corrosive environment that exceeds an hour, as needed in many applications. Finally, most of the studies have focused on corrosion at room temperature, whereas the performance of such surfaces in corrosive environments at higher than room temperature is not reported.

The goal of the present study is to address the aforementioned limitations by considering the fabrication and corrosion performance of superhydrophobic copper surface. A facile, rapid process of electrodeposition of copper is presented with fabrication times less than 5 minutes at a very low overpotential of –1.1 volt that reduces the energy requirement for fabrication. The as-fabricated cauliflower shaped multiscale textured surfaces were chemically modified (functionalized) using stearic acid, an environmentally benign fatty acid. Corrosion characteristics of the fabricated surfaces were measured using electrochemical impedance spectroscopy as well as the linear polarization technique to elucidate insights into the corrosion

mechanism on superhydrophobic surfaces. Systematic studies are conducted to quantify the effects of functionalization time (t_f), corrosivity of the immersion medium, immersion time, and temperature on the corrosion performance of as-purchased copper and textured superhydrophobic copper surfaces. The corrosion characteristics are investigated over the range of extremes of corrosivity, from a harsh acid medium with a pH of 1 to a harsh alkaline medium, pH = 14, including a 3.5% NaCl as a simulation for the marine environment. The study also reports corrosion measurements for long immersion time in a harsh environment via an *in situ* linear polarization method. Additionally, corrosion studies are presented, for the first time, on a range of temperatures in the range of 23°C–90°C, from which an Arrhenius model is developed for the temperature-dependent corrosion rate of the superhydrophobic surfaces.

The article is organized as follows: the experimental methods of fabrication and characterization are described in the next section. The results of the study are presented and discussed in Section 3 in terms of the corrosion parameters as function of surface functionalization time, pH of the immersion environment, immersion time and immersion temperature. The principal conclusions of the study are summarized in Section 4.

2. EXPERIMENTAL METHODS

2.1. Materials and reagents.

Plain multipurpose copper sheet was purchased from McMaster, USA. Analytical-grade copper sulfate ($CuSO_4$, 99+%), sulfuric acid (H_2SO_4), acetone (99.5+%), methanol (99.8+%), and stearic acid ($CH_3(CH_2)_{16}CO_2H$, 97%) were purchased from Fisher Scientific, (Pittsburgh, PA, USA) and used as received without any further purification. For the preparation of aqueous solutions, deionized (DI) water with 14MΩ.cm resistance was purchased from CQ Concept (Illinois, IL, USA).

2.2. Fabrication of copper superhydrophobic surfaces.

A three-electrode electrochemical experiment setup, shown schematically in Figure 1, was used for the facile electrodeposition of copper on the copper substrate [32]. As purchased copper sheets were used as working and reference electrodes, while a platinum mesh was used as the counter electrode. An AUTOLAB PGSTAT128N potentiostat (ECO Chemie, Utrecht, The Netherlands) was used for all electrodeposition experiments. Using a mixture of 1M $CuSO_4$ and 0.5M H_2SO_4 as the electrolyte, electrodeposition was done over one side of the working

electrode while the other side was covered from electrodeposition with 3M® painting tape. All the surfaces used in the electrodeposition experiments were sonicated in acetone for 10 minutes, rinsed with DI water and dried in a nitrogen stream. Before each electrodeposition, the electrolyte was de-aerated by bubbling pure nitrogen gas for at least 20 minutes.

The distance between the working and the reference electrodes was set to 0.5 cm. Negative overpotentials ranging from -0.5 V to -1.1 V in steps of -0.2 V were used for electrodeposition. For cases of -0.9 V and -1.1 V, which lead to an aggressively multiscaled texture of the deposited layer, a second deposition was conducted right after the first electrodeposition by applying -0.15 V for 10 seconds. The second deposition helps adhere the multiscale electrodeposited layers together and prevent them from peeling off the surface [32]. The electrodeposition time at each overpotential voltage was calculated to obtain about 30-micrometer deposition thickness (h) as per the relationship: $h = \frac{QM}{nF\rho A}$, where F is the Faraday constant, A is the surface area of the deposition, ρ is the density of the deposited copper, Q is the charge transferred in coulomb throughout the deposition ($Q = i.dt$), M is the molar weight of copper, and n is the number of transferred electrons in the copper reduction reaction, $Cu^{2+} + 2e^- \rightarrow Cu$.

After each electrodeposition run, the as-fabricated sample was rinsed with acetone and DI water and dried in a pure nitrogen stream. The fabricated samples were then vacuum dried at room temperature for 24 hours before the surface modification step to lower the surface energy. The electrodeposited textured surfaces were functionalized by immersing the samples in a solution of 0.02 M stearic acid (STA), an environmentally benign fatty acid, in methanol at room temperature, as depicted in Figure 1. The functionalizing time was varied between 1 h to 72 h as part of the systematic study to determine its influence on the corrosion behavior. in modification solution at room temperature. The fabricated superhydrophobic surfaces demonstrated excellent water repellency with high contact angle, as seen in Figure 1.

2.3. Morphology, chemical composition analysis, and wettability characterization.

The surface chemical composition was analyzed in a VersaProbe III Scanning XPS Microprobe (Physical Electronics, U.S.A.), using a monochromatic AlKα X-ray source (1486.6 eV) at 100 W. Images of the deposited surface morphologies and the elemental analysis of the surfaces were obtained with a field-emission scanning electron microscope (SEM) (JEOL 2100, Japan), operating at an acceleration voltage of 15 kV connected to energy dispersive x-ray

analyzer (OXFORD, UK). The intrinsic wettability of water on the surfaces was characterized by measuring contact angle using a goniometer (ramé-hart model 590, NJ USA), at five different positions on each sample. The roll-off angle was measured by the same apparatus with 25 µl deionized (DI) water and tilting cradle method. For wettability characterization after each immersion test, the coupons were first slightly washed using a hand-squeezed laboratory DI-water bottle and left to dry in room atmosphere overnight before the contact angle measurement.

2.4. Corrosion inhibition characterization.

All the samples studied for corrosion inhibition were fabricated at -1.1 V overpotential and functionalized in 0.02 M stearic acid solution. Electrochemical three-electrode tests were carried out to measure and characterize the corrosion inhibition properties of the samples. Ag/AgCl (NaCl saturated) served as a reference electrode placed a distance of less than 3 mm from the sample surface (working electrode) in order to minimize the effect of solution resistance. A Pt mesh placed equidistant to the two other electrodes was used as a counter electrode. Potentiodynamic polarization (PDP) curves, electrochemical impedance spectroscopy (EIS) test and linear polarization (LP) test data were recorded with a potentiostat device Solarton Inc. (model 1240 PA, USA) equipped with a frequency response analyzer. A scan range of -300 mV to +300 mV with respect to open circuit potential and a scan rate of 1 mV/s was used for the PDP test, while a 1/6 V/h scan rate, as per ASTM G3-14 (2019) standard [40], was used for the LP tests. Impedance spectra were registered in a range of 0.05 Hz to 100 kHz with sinusoidal signals of 10 mV amplitude with respect to the open circuit potential.

It is known that the open circuit potential (OCP) needs an initial time for stabilization and that this time is specific to the environment and the studied metal alloy [41]. Since corrosion is based on redox reactions happening at the surface, the very surface chemistry undergoes changes over time causing possible potential drift. To determine the stabilization time, the open circuit potential (OCP) was recorded in 3.5% NaCl solution at room temperature for bare copper, as the control sample, and the superhydrophobic copper surfaces. A higher relative potential fluctuation was seen in the first 10 minutes for the superhydrophobic copper samples that stabilized after about 20 minutes. Furthermore, the bare copper control sample potential drifted lower with a higher gradient after about 60 minutes, which was sought to be avoided. Based on these observed variations of the OCP with time, a 30-minute stabilization time in the electrolyte was selected before conducting each of the corrosion tests.

The data obtained from PDP scans were used to construct Tafel plots for determination of the corrosion potential, E_{corr}, corrosion current density, j_{corr}, and the corrosion resistance, R_{corr}. The EIS data were analyzed by constructing an equivalent electrical circuit model from which the charge transfer resistance, R_{ct}, was calculated using the Zview® software (Scribner Associates, Inc., NC, USA). The analysis of the obtained data is discussed in detail in the following section. The corrosion tests were conducted to systematically study and quantitatively assess the effects of the functionalization time, corrosivity of the environment in terms of pH, long term immersion time, and temperature as discussed in the next section.

3. RESULTS AND DISCUSSION

The results of the study are presented and discussed in this section, in terms of the morphology and wettability of the fabricated superhydrophobic surfaces, the chemical composition of the functionalized surface of the superhydrophobic surfaces, and the corrosion inhibition characteristics of the superhydrophobic surfaces relative to a bare copper surface.

3.1. Morphology, wettability, and chemical composition.

The surface morphology of the electrodeposited surfaces before functionalization is depicted in Figure 2(a)–(d), for deposition voltages ranging from -0.5 V to -1.1 V, where a clear trend in the development of multiscale asperities with respect to the electrodeposition overpotential is evident. At a low overpotential voltage of 0.5 V, Figure 2(a), the deposition is relatively smooth with little surface roughness. An increase in the deposition overpotential to 0.7 V reveals the emergence of semi-spherical asperities on the surface, as seen in the SEM image of Figure 2(b). At higher overpotentials, 0.9 V and 1.1 V, the growth rate of deposition increased significantly. Figure 2(c) and 2(d) show the multiscale, cauliflower-shaped asperities deposited on to the copper surface at 0.9 V and 1.1 V, respectively.

As discussed earlier, theoretically, the two factors which play the major role in turning a surface to a hydrophobic or superhydrophobic surface are the surface roughness and the surface energy. The surface energy of the electrodeposited samples was lowered by functionalization them in a 0.02 M stearic acid solution in methanol for 1 hour. After that, the surfaces were characterized for their wetting contact angle with respect to a 10 μl DI-Water sessile drop, as depicted in the insets in Figure 2(a)–(d) which reveal the interplay between the roughness, functionalization and the non-wetting characteristic of the surface. Figure 2(a) shows a contact

angle of 133 degrees for the surface electrodeposited at 0.5 V; with the emergence of the semi-spherical asperities at 0.7 V overpotential, the contact angle is seen to increase by about 14 degrees to 147 degrees in Figure 2(b). Surfaces fabricated at an overpotential of over 0.9 V reveal distinct superhydrophobicity with static contact angle larger than 150° and up to 160° for an overpotential of 1.1 V in Figure 2(d). In the 0.9 V and 1.1 V overpotential cases, the measured contact angle hysteresis was below 5° signifying excellent non-wettability of the fabricated surfaces. Moreover, the roll-off angle test showed a high average roll-off angle of 41 ± 30 and 36 ± 27 degrees for the 0.5 V case 0.7 V cases, respectively, while this value was below 5° for 0.9 V and 1.1 V cases. Figures 2(a)–(d) clearly demonstrate the combined role of the multiscale asperities and low surface energy in causing superhydrophobicity, that either alone will not produce.

In order to identify the main chemical composition of the superhydrophobic copper surface, X-ray photoelectron spectroscopy (XPS) scans were recorded on the samples fabricated at an overpotential of -1.1 V with a functionalization time, t_f, of 24 h in 0.02 M stearic acid solution in methanol. A functionalization time of 24 h was selected for the XPS analysis so as to provide substantial stearic acid layer for the investigation**.** Figure 2(e) shows the XPS trace, from which carbon, oxygen, and copper are identified as the main components of the surface. The carbon and oxygen peaks indicate the successful reaction and bonding of stearic acid with the rough copper surface. Figure 2(f) highlights the variation in the range of 930–950 eV and shows a broad Cu 2p 3/2 feature which can be deconvoluted into two peaks at 932.6 and 934.8 eV (E_b), and a characteristic satellite feature for Cu (II) at 940-945 eV. The minor peak at 932.6 eV can be assigned to Cu_2O, while the major peak at 934.8 eV can be assigned to $Cu(OH)_2$ [42]. The Cu $L_3M_{45}M_{45}$ Auger feature exhibits a single peak with a kinetic energy of 915.0 eV (E_k). The Modified Auger Parameter of 1849.8 eV ($E_b + E_k$) for the major peak at 934.8 eV is in good agreement with the value of $Cu(OH)_2$ (1851.3 eV) [42], confirming the major presence of $Cu(OH)_2$ on the surface. Since the minor 932.6 eV peak was not observed after the first sweep and accumulated after repeated sweeps, Cu_2O species could be resulted from reduction of $Cu(OH)_2$ after prolonged X-ray exposures. All these mean that the Cu is primarily in the form of CuO or $Cu(OH)_2$, suggesting $Cu_2O + 2CH_3(CH_2)_{16}COOH \rightarrow 2Cu[CH_3(CH_2)_{16}COO] + H_2O$ as a possible reaction mechanism for chemisorption of stearic acid with the surface cupreous oxide [18].

3.2. Effect of functionalization time on corrosion.

Parametric tests were done to investigate the effect of functionalization time, t_f, on the corrosion inhibition behavior of superhydrophobic copper surfaces immersed in solutions ranging from the extremely acidic (pH = 1) through the near-neutral 3.5% NaCl solution ($pH \approx$ 7) to the extremely alkaline (pH = 14). The solutions with extreme acidity (pH = 1) and extreme alkalinity (pH = 14) were prepared by hydrolysis of sulfuric acid and sodium hydroxide in DI-water, respectively. In each case, the functionalization time in the fabrication of the superhydrophobic surfaces was varied in the range of $t_f = 1$ h to $t_f = 72$ h and, for comparison, bare copper samples were also immersed in the solutions. The static contact angles of DI-water on the 1.1 V overpotential electrodeposited copper surfaces with 1 hour functionalization time and beyond was 160 ± 4.1 degrees with roll-off angles below 5 degree. In comparison, for the bare copper surface, the static contact angle and the roll-off angle was measured as 88.7 ± 5.7 and 48.0 ± 5.5 degrees, respectively. Note that unfunctionalized electrodeposited copper surfaces has shown superhydrophilicty with a low contact angle The studies in this parametric set were conducted at a temperature of 23°C (the actual room temperature in the laboratory) and consisted of potentiodynamic polarization tests as well as electrochemical impedance spectroscopy, as discussed below.

Reviewer 1; Comment 3

Reviewer 1; Comment 5

Potentiodynamic polarization (PDP)

Figure 3(a) shows the potentiodynamic polarization (PDP) data recorded for bare copper and superhydrophobic copper surfaces with six different functionalization time, at a temperature of 23°C. It is seen that, in general, the corrosion current density decreases with increasing functionalization time, and that all of the functionalized samples have a distinctly lower current density compared to bare copper, as evident in the progression of the curves from (a) to (g) in Figure 3. In order to quantitatively deduce the corrosion parameters from the measured PDP data, a Tafel extrapolation method was used, where the slope of the linear part of the cathodic region (β_{cat}) and anodic region (β_{an}), in mV/decade, were determined as illustrated in Figure 3(a) for the case of bare copper. From these slope measurements, the corrosion voltage, E_{corr}, and current density, j_{corr} ($\mu A \cdot cm^{-2}$) were derived from the intersection of the two linear asymptotes, and the corrosion resistance, R_{corr} ($\Omega \cdot cm^2$) was estimated from the parameters extrapolated from the Tafel plots by the Stern-Geary equation, $R_{corr} = \frac{\beta_{an} \cdot \beta_{cat}}{2.303 \cdot (\beta_{an} + \beta_{cat}) \cdot j_{corr}}$ [43].

Note that the Stern-Geary relationship is strictly valid when both the anodic and cathodic reactions follow the Tafel kinetics. Even though the Stern-Geary equation has been used in the literature to analyze copper foil and superhydrophobic surfaces [44, 45], and there was no dissolution of copper noted in the present study, the R_{corr} values are not used here as the sole basis of the corrosion inhibition analysis, rather as an estimate for relative comparison in the parametric tests. Moreover, the estimated values of R_{corr} are shown later in the article to correlate closely to the charge transfer resistance measured from electrochemical impedance spectroscopy methods.

The corrosion current density, j_{corr}, corrosion voltage, E_{corr}, corrosion resistance, R_{corr}, and the corrosion rate, CR, calculated from the PDP measurements are summarized in Figures 3(b)–(d). Figure 3(b) presents the variation of the corrosion current density, j_{corr}, and the corrosion voltage, E_{corr}, with functionalization time for superhydrophobic surfaces and for bare copper, as reference, for the three different solutions studied (pH values of 1, ≈ 7 (3.5% NaCl), and 14). For each pH value considered, the corrosion current is decreases from bare copper to the superhydrophobic surface and decreases monotonically with increasing functionalization time for the superhydrophobic surfaces. The corrosion voltage, E_c, however, is seen to increase slightly from bare copper to superhydrophobic surfaces, but remains relatively insensitive to the functionalization time among the superhydrophobic surfaces. The corrosion inhibition effect of the fabricated superhydrophobic surfaces is evident in Figure 3(b) in two ways. First, the positive shift in the corrosion potential and second, the decrease in the corrosion current density which together correspond to a lower corrosion rate. For example, for immersion in the 3.5% NaCl solution, it is seen that E_{corr} increases +75.12 mV (-0.229 mV to -0.154 mV) for the sample functionalized for 1 h compared to the bare copper control sample. As the functionalization time increased, a net change of +10.29 mV ($E_{corr} = -0.219$ mV) is observed for the 72 h functionalized sample relative to the bare copper surface. Overall, the superhydrophobic surfaces exhibit a noble potential compared to the copper control samples, over the entire range of solution pH values.

On the other hand, for the 3.5% NaCl solution, the corrosion current density is seen to decrease significantly to 6.55 $\mu A.cm^{-2}$ for 1 h functionalization time—about one third of the current density value of 1.96 $\mu A.cm^{-2}$ for the bare copper control sample. Figure 3(b) further

reveals that the current density decreases dramatically with an increase in functionalization time: about one order of magnitude reduction in j_{corr} of 0.48 $\mu A.cm^{-2}$ is achieved for the samples functionalized for 4 h, and the current density is as low as 0.15 $\mu A.cm^{-2}$ for the 72 h functionalization time. More dramatic reduction in the current density by three to four orders of magnitude is also seen in Figure 3(b) for the samples immersed in $pH = 1$ and 14: the current density decreases from 8.85 $\mu A.cm^{-2}$ (bare copper) to 0.0027 $\mu A.cm^{-2}$ (72 h functionalization) for immersion in an extremely acidic, $pH = 1$, solution, and from 404 $\mu A.cm^{-2}$ (bare copper) to 0.028 $\mu A.cm^{-2}$ (72 h functionalization) for immersion in an extremely alkaline, $pH = 14$, solution. Such low corrosion current density values clearly indicate the effective anti-corrosive nature of the fabricated superhydrophobic surfaces. Expectedly, therefore, the corrosion resistance, R_{corr}, increases for the superhydrophobic surface compared to the bare copper surface in Figure 3(c), and with the functionalization time among the superhydrophobic surfaces, for all the solution pH studied. The resistance is seen to increase over 287-fold to 1658 $k\Omega \cdot cm^2$ for the superhydrophobic sample with 72 h functionalization immersed in 3.5% NaCl solution, compared to the 5.77 $k\Omega \cdot cm^2$ for a bare copper surface immersed in the same solution concentration. For $pH = 1$ and $pH = 14$, the corresponding resistance increase is seen to be from 1.50 $k\Omega \cdot cm^2$ to 3,688 $k\Omega \cdot cm^2$ and from 0.06 $k\Omega \cdot cm^2$ to 114.32 $k\Omega \cdot cm^2$.

The two- to four-orders of magnitude decrease in the current density noted in Figure 3(b) of superhydrophobic copper surfaces can be attributed to multiple mechanisms. The fabricated superhydrophobic surfaces include a chemisorbed functionalization layer which prevents the electrolyte, including the halide anions (Cl^-), from reaching the copper surface and acts as a physical barrier to avert oxidation of the surface. In addition, the superhydrophobicity of the samples ensures the presence of air bubbles trapped in the interasperity regions of the multiscale surface microstructures that serve to cushion the electrolyte further away from the surface, thereby limiting the potential for corrosion. Corrosion is a surface phenomenon in nature that begins from microcavities which have higher local current densities, which, combined with the water repellency effect of the SHS, can explain the trend in the improvement of the corrosion inhibition of the prepared samples with an increase in functionalization time. As the time of immersion in stearic acid solution increases, the number of micro-size defects, defined in terms of deviation from homogeneous chemisorption of the stearic acid, decreases. Therefore, there are fewer possible pairs of reduction and oxidation sites available to the electrolyte on the surface

with an increase in functionalization time.

In a general metal cathodic corrosion reaction, $M \rightarrow M^{n+} + n \cdot e^{-}$, the rate of corrosion can be calculated by relating the current flow to mass of metal being corroded, m, in terms of the Faraday constant (F), as: $Q = nF(m/A_w)$, where Q is the transferred charge, n is the number of electrons transferred per molecule or atom of metal and A_w is the atomic weight of the metal. By defining an equivalent weight (EW) as $\frac{A_w}{nF}$ and taking the time derivative of the expression for Q, the corrosion rate ($CR = \frac{1}{\rho A} \cdot \frac{dm}{dt}$) in mm/y (denoted as mmPY) is obtained as $CR = 3276.6 j_{corr} E_w/\rho$ where $j_{corr} = \frac{1}{A} \cdot \frac{dQ}{dt}$ is the current density, ρ is the metal density and A is the metal surface area being corroded. Figure 3(d) presents the variation of the corrosion rate with the functionalization time of the superhydrophobic surfaces in comparison to the corrosion rate of bare copper surface, in the three different pH solutions. The corrosion rate curves follow the same variation as that of the current density in Figure 3(b), and decrease significantly as the functionalization times increases. This decrease is observed to be about two to four orders of magnitude for $pH = 1$ and $pH = 14$, for the samples with a functionalization time of 24 h and above. For the samples immersed in 3.5% NaCl ($pH \approx 7$) the corrosion rate decreases by nearly two decades. In all the cases, the distinct corrosion inhibition benefit of the superhydrophobic surfaces is evident relative to bare copper surface, which may be quantified further in terms of a corrosion inhibition efficiency, defined as $\eta_c = \left(1 - \frac{j^{SH}}{j^0}\right) \times 100\%$, where j^0 and j^{SH} are the corrosion current density for the bare copper and the superhydrophobic surfaces, respectively. In all the three solution pH studied, the samples with 8 h functionalization time had >90% corrosion inhibition efficiency. This value is over 99% for pH = 1 and pH = 14, and over 95% for 3.5%NaCl (pH ~ 7) solution for samples with functionalization time of 24 h and above. The dynamic polarization curve extrapolated information including β_{an}, β_{cat}, j_{corr}, E_{corr}, η are summarized and tabulated in Table 1.

Electrochemical impedance spectroscopy (EIS).

The corrosion of bare copper and superhydrophobic copper samples functionalized at the six different times, were also studied using the electrochemical impedance spectroscopy (EIS) technique, for immersion in 3.5% NaCl and solutions of $pH = 1$ and $pH = 14$, at a temperature of 23°C. Figure 4 presents the measured data on corrosion in 3.5% NaCl, as the various markers,

in terms of the Nyquist plots for the bare copper sample (Figure 4(a)) and the superhydrophobic samples (Figure 4(b)), as well as the Bode plot (Figure 4(c)) and the phase plot (Figure 4(d)) for all the samples studied. The Nyquist plots for the functionalized superhydrophobic copper surfaces (Figure 4(b)) are distinctly different in shape and size compared to the bare copper surface (Figure 4(a)), which correspond to a difference in the corrosion mechanism between the two. The Nyquist plot for the bare copper sample shows a semicircle at the high-frequency region and a linear variation with a slope of ~45 degrees in the low-frequency region. The semicircular head of the plot is an indicator of charge transfer at the surface and the linear tail is an indicator of the presence of mass transfer (diffusion) attributed to either of the following transports: (1) the diffusion of anions produced from the reduction of the copper in the presence of the electrolyte, which diffuses halide copper complexes, namely $CuCl_2^-$ or $CuCl_4^{2-}$, into the bulk solution or (2) the diffusion of the dissolved oxygen toward oxidation corrosion sites on the surface [7,8]. In contrast, the mass transport region at the low frequency is absent for the superhydrophobic surfaces in Figure 4(b) suggesting an absence of or an insignificant transport of redox species. Furthermore, among the superhydrophobic surfaces in Figure 4(b), the diameter of the capacitive loop increases with an increase in functionalization time indicative of a significant lower charge transfer for these surfaces in comparison to the bare copper surface.

The Bode diagram in Figure 4(c) provides further evidence of the corrosion behavior among the bare and the superhydrophobic samples. It is seen that the Bode plots shift toward higher a impedance modulus over the entire scanned frequency range for the superhydrophobic surfaces compared to bare copper, with generally increasing values with functionalization time among the various superhydrophobic samples studied. It has been reported that the impedance modulus value in the low-frequency region of the Bode diagram may be regarded as an indicator of the corrosion inhibition behavior [10,11]. The impedance magnitude at a frequency of 0.05 Hz, for the superhydrophobic sample functionalized for 1h is seen to be about an order of magnitude larger than the corresponding value for the bare copper sample. With increasing functionalization time from 24 h to 72 h, the impedance value is seen to increase by a further order of magnitude, resulting in a two-orders of magnitude increase for the superhydrophobic surface with 72 h functionalization relative to bare copper.

Collectively, the Nyquist and the Bode plots in Figures 4(a)–4(c) confirm a greater corrosion inhibition in the case of the functionalized superhydrophobic surfaces, and an increasing

corrosion resistance with increasing functionalization time. Additionally, the phase plot in Figure 4(d) presents the variation of the negative of the phase angle with frequency for all the samples considered. In general, the variations exhibit a nonmonotonic trend with a peak phase angle at certain frequencies. The peak angle is larger and shifts to the higher frequencies for the longer functionalization times. Of further note in Figure 4(d) is the presence of two capacitive peaks for the functionalized samples that are especially evident in the case of the longer functionalization times.

Electrochemical impedance spectroscopy (EIS) data recorded on immersion of bare copper and superhydrophobic copper surface functionalized for 24 h in solutions with $pH = 1$ and $pH = 14$ are presented in Figure 5 along with the data for the 3.5% NaCl solution, redrawn from Figure 4 for comparison. In the Nyquist plots of Figure 5(a,b), the imaginary axis to the real axis scale ratio is kept to 3:1 for each pH value, for clarity of the shape of the curves. The data correspond to a temperature of 23°C. For immersion of bare copper in the extremely acidic and the extremely alkaline solutions, the Nyquist plot in Figure 5(a) does not show a distinguishable diffusion tail (a slope of approximately 45° near the origin) in the low-frequency region that is evident for the data on the 3.5% NaCl solution. For the 24 h functionalized samples in all the pH cases, Figure 5(b) shows that the capacitive loops corresponding to the double-layer capacitance are much larger in magnitude and extend longer than the respective data for the bare copper control sample in Figure 5(a). This indicates excellent corrosion inhibition performance of the superhydrophobic surfaces over the entire range of pH values. Furthermore, the Bode plots in Figure 5(c) show that the impedance magnitude is consistently at least a decade larger for the superhydrophobic surface over the entire frequency range and for all pH values. At the frequency of 0.05 Hz, the one, two and three orders of magnitude increase in the impedance magnitude for $pH = 14$, $pH \sim 7$ (3.5%NaCl), and $pH = 1$, respectively, offer evidence of the great corrosion inhibition characteristics of the superhydrophobic surfaces. The phase plots in Figure 5(d) show similar characteristics to that seen for the 3.5% NaCl solution in Figure 4(d), in the presence of a peak phase angle for immersion of bare copper in $pH = 1$ and $pH = 14$ solutions, with the latter demonstrating a double peak. For the superhydrophobic surface, the peak angle is shifted to larger frequencies, uniformly for all solution pH values. Furthermore, a twin capacitive peak is evident for immersion in all the solutions.

The observations in Figures 4 and 5 and are used to construct an equivalent circuit model for

the corrosion of the bare and superhydrophobic surfaces, in order to determine the parameters describing the corrosion of the surfaces in the different pH solutions. Before constructing the equivalent circuit model, the validity of the EIS measurement was tested via Kramers-Kronig (K-K) analysis [46] to ensure that the EIS data represent the physical processes of the electrochemical system studied [47]. The Nyquist and the phase plots for bare copper (Figures 4(a), 5(a) and 4(d), 5(d)) suggest the use of a Warburg diffusion element in the circuit. Moreover, the semi-circular arcs in the Nyquist plots (Figures 4(a), (b) and 5(a), (b)) for both functionalized and bare copper samples suggest the use of a capacitor in parallel with a resistor. However, as seen in the phase diagram, Figures 4(d) and 5(d), the peaks do not reach the –90 degree value, the phase angle of an ideal capacitor. The depressed semi-circles in Figure 4(a), 5(a) and 4(b), 5(b) are known to be due to the dispersing effect [48] and may be effectively modeled by a constant phase element (CPE), instead of a pure capacitor, in parallel to a resistor. The use of CPE is well established in the literature and serves to compensate for the non-homogeneity of the systems arising from such factors as roughness, porosity, reactivity, potential, and current distribution attributed to the interface or the electrode geometry [49, 50]. Furthermore, the presence of two capacitive peaks in the phase plots for the superhydrophobic surfaces, Figures 4(d) and 5(d), justifies the use of two CPEs in the equivalent circuit model. Experimental observations and the measured data suggest the existence of a concentrated layer of dissolved corrosion redox species in the vicinity of the bare copper surface in the electrolyte, which has been treated as a film in its correspondent equivalent circuit. Likewise, a Warburg element was used in series with the charge transfer resistor to compensate for the diffusion effect and the observed low-frequency tail.

With the foregoing considerations, equivalent resistive and capacitive circuits are constructed for the bare copper and the superhydrophobic copper surfaces, as presented in Figure 6(a) and 6(b) for the bare copper and superhydrophobic surfaces, respectively. The equivalent circuits comprise the following elements: R_s representing the solution resistance, R_f denotes the surface film resistance to corrosion, R_{ct} is the charge transfer resistance corresponding to corrosion inhibition resistivity of the surface, and $\mathrm{CPE_f}$ and $\mathrm{CPE_{dl}}$ as the constant phase elements for the film and double layer, respectively, defined as $CPE_i = \frac{1}{Q_i(j\omega)^{n_i}}$, where j is the imaginary number $(= \sqrt{-1})$, ω is angular frequency, the subscript i denotes either the surface film (f) or

the double layer (dl), and Q_i and n_i are the magnitude of the capacitance and the phase exponent in the respective layer, such that a capacitor is an ideal CPE with a phase exponent of 1. The experimental data measured using EIS for immersion of the bare and the superhydrophobic samples (with the different functionalization times) in the three solutions were fit to the respective equivalent circuits, as shown by the solid lines in Figures 4 and 5. The corresponding calculated circuit element parameters, tabulated in Tables 2 and 3, demonstrated the following salient features:

(1) the Q_f values for the superhydrophobic surfaces (0.006–0.02 for $t_f = 72$ h, for example) were generally one to three orders magnitude smaller than the corresponding values for bare copper (14.36–678.54), for all solution pH values. A higher Q_f means a higher level of penetration of the corrosive solution into the film cavities, and a constant decrease was seen in this value with an increase in the functionalization time.

(2) the Q_f values were all lower than Q_{dl} values for all surfaces, and for all solution pH values, implying that the charge double layer effect is a dominant corrosion phenomenon.

(3) the Q_{dl} values for superhydrophobic surfaces functionalized for 72 h were 0.4 ($pH = 1$), 2.75 (3.5% NaCl) and 1.37 ($pH = 14$), which were at least three decades lower than the corresponding values of 711.81, 167.07, and 3,211.10 for the bare copper surface. This trend is consistent with the expectation of less penetration of the solution into the double layer for the superhydrophobic surfaces. Furthermore, Q_{dl} for the bare copper immersed in extremely acidic and the extremely alkaline conditions are significantly higher values compared to the near-neutral 3.5% NaCl solution, reflecting the fact that a harshly acidic or alkaline condition can increase the penetration of the solution. However, with functionalization, the Q_{dl} for the superhydrophobic surface decreases signifying a protection.

(4) The values of the film resistance, R_f, which can be interpreted as a physical barrier against corrosion, ranged from 0.01–540.00 $k\Omega \cdot cm^2$ and were much smaller than the R_{ct} values of 0.04–1930.00 $k\Omega \cdot cm^2$, for both bare copper and superhydrophobic surfaces alike, and in all pH environments. The relative magnitude of the two resistances is consistent with the observation from the PDP studies that the main contributor to corrosion inhibition is the superhydrophobicity effect rather than the physical barrier mechanism.

Figure 6(c) presents the variation of the charge transfer resistance (R_{ct}) values of the

equivalent circuits for the bare copper and the superhydrophobic surfaces as a function of the functionalization time. The charge transfer resistance R_{ct} is seen to increase from the bare copper to the superhydrophobic surface, and further, increases monotonically with the functionalization time. Among the three different pH environments studied, the resistance is nearly independent of pH for $pH \lesssim 7$, but decreases with further increase in pH from 7 to 14. Of particular note is that the R_{ct} values for the different surfaces and the solution pH values closely match the corresponding R_c values derived from potentiodynamic test results, as presented in Figure 3(c), and follows the trend well. The close correspondence of the R_{ct} and R_{corr} values provides validation of the developed equivalent circuit model, which may be used for a deeper insight into the corrosion inhibition mechanism of the studied surfaces.

The corrosion inhibition seen in Figures 3–6 is explained by three phenomena [51, 52]. First is the passivation of the active corrosion sites by the chemisorbed functionalization agent molecules acting as physical barrier preventing the redox cations and anions from reaching the metallic surface. The second mechanism is the existence of excessive similar charge on the surface which presents repulsive forces that retard the diffusion of the corrosion redox species toward the surface. The pH effect on surface charge on superhydrophobic surfaces may provide insight into the second corrosion inhibition mechanism. It is shown experimentally in multiple studies that the interface of air/electrolyte on hydrophobic surfaces is basic at pH above the isoelectric point (IEP), the pH at which particular molecules carries no net electric charges in the solution [53-55]. For hydrophobic surfaces, the IEP is $pH = 2\ to\ 4$ [53, 55]. Further, it is also known that the OH^- ions have the highest absorption energy toward the water/SHS interface followed by Cl^- and H^+ [53], independent of the existence of multivalent anions in the electrolyte such as$CuCl_3^{2-}$ or Cu^{2+}[54, 55]. The second mechanism for the pH cases studied has been detailed as follows:

- For $pH = 1,$ the $pH < IEP$ and the electrolyte/SHS interface is positively charged. Due to abundance of hydronium ions at this pH, the cathodic corrosion reduction reaction in the acidic environment follows the $O_2 + 4H^+ + 4e^- \rightarrow 2H_2O$ pathway rather than $O_2 + 2H_2O + 4e^- \rightarrow 4OH^-$. The positive charge at the interface exerts a repulsive electrostatic force retarding H^+ from diffusion to the interface and hence improves the corrosion resistance.

- For pH ~ 7, 3.5% NaCl solution, the $pH > IEP$ and the electrolyte/SHS interface carries OH^- static electric charge. In the presence of sodium chloride the anodic corrosion reaction follows one of the (I) $Cu + Cl^- \rightarrow CuCl + e^-$ or (II) $CuCl + Cl^- \rightarrow CuCl_2^-$ pathways. Therefore, the negative excessive charge retards the corrosion redox reaction and act as an anti-corrosion mechanism specific to hydrophobic surfaces.
- For $pH = 14$, the $pH > IEP$ and the electrolyte/SHS interface is negatively charged. The $O_2 + 4H^+ + 4e^- \rightarrow 2H_2O$ cathodic corrosion pathway is less favorable in this case, and the electrolyte is deprived of hydronium (or H^+) by 13 orders of magnitude compared to the basic case ($pH = 1$) and by 7 orders of magnitude compared to the chlorine case ($pH \sim 7$). Contrary to the other two cases, the excessive charge, therefore, neither retards nor accelerates corrosion on the surface. As a result, the corrosion resistance is generally lower in the harshly basic environment compared to the acidic environment in Figure 6(c).

The third and the most important corrosion inhibition mechanism that plays the major role compared to the other two, namely physical barrier and surface charge, is the existence of an air/electrolyte interface. The stable air bubbles between the multiscale porous structure of the superhydrophobic and the electrolyte, forms a cushion of air, with which reduces the number of the available redox reaction pair sites for corrosion to initiate.

3.3. Long term immersion and corrosion inhibition stability.

The results reported so far were for bare copper and superhydrophobic surfaces immersed in the different pH solutions for 30 min. In order to characterize the stability of the corrosion inhibition of the fabricated superhydrophobic surfaces, immersion tests were conducted for relatively longer durations of up to 800 min (referred to as "long term" in this study, which differs from the studies in the literature that refer to long term in duration of several days) in extremely acidic ($pH = 1$), near-neutral halide (3.5% NaCl, $pH \approx 7$) and extremely alkaline ($pH = 14$) solutions at room temperature ($23°C$). Linear polarization tests were performed intermittently at periodic intervals during the course of the immersion duration to derive the corrosion parameters, E_{corr}, j_{corr}, R_{corr}, and the corrosion rate (CR). With overpotential of ±20 mV with respect to open circuit potential, that are about 12 times smaller than the overpotential in a potentiodynamic polarization test, linear polarization tests are relatively nondestructive in nature. The corrosion potential, E_{corr}, is obtained as the intersection of the $j = 0$ A/cm^2 line and

the measured voltage-current density data. A linear line was fit to the data at ±10 mV of the E_{corr} The slope of the fitted line is the corrosion resistance, R_{corr}. The anodic and cathodic slopes, β_{an} and β_{cat}, were estimated by fitting Tafel relationship to the measured data, and the corrosion current was derived from the Stern-Geary relationship. Even though there was not a significant dissolution of copper found for superhydrophobic samples in the present study, it should be noted that the corrosion resistance values derived from Stern-Geary equations are only used as an estimate for a relative comparison, as discussed in section 3.2.

The corrosion resistance and the corrosion rate are summarized in Figure 7 for the long-term immersion tests in the three pH solutions, where the solid markers correspond to bare copper and the open markers denote the parameters for a superhydrophobic surface with a functionalization time of 24 h. Figure 7(a) shows that the corrosion resistance for the superhydrophobic surface is stable throughout 800 minutes of immersion time and is consistently higher than the values for bare copper in all the three pH environments. For $pH = 14$, a reduction in the corrosion resistance is noted with the immersion duration, although the corrosion resistance of the superhydrophobic surface remains higher than that for bare copper throughout the duration of the test. Figure 7(b) presents the variation of the corrosion rate with immersion time and demonstrates excellent stability, that may be examined in terms of a corrosion inhibition efficiency, as defined in section 3.2. The corrosion inhibition efficiency stays at over 99% throughout the test for the 3.5% NaCl solution; for $pH = 1$ the corrosion efficiency begins at 99.9% efficiency and drops slightly to 96% by the end of the test, which is still an excellent corrosion inhibition compared to bare copper surface. For $pH = 14$, the corrosion inhibition efficiency remains stable at about 95%. Note that since the corrosion rate is a linear function of j_{corr}, the trends in Figure 7(b) on the corrosion rate may equivalently be interpreted to be the same as that in the corrosion current density.

The impact of the long-term corrosion of the samples was further assessed by means of scanning electron microscopy (SEM) imaging of the surfaces, composition analysis using energy dispersive x-ray (EDX) technique, and contact angle measurements as presented in Figure 8. Figures 8(a)–8(c) show the SEM images of the superhydrophobic surface with a functionalization time of 24 h, at three different magnifications, prior to the long term corrosion test. Figures 8(d)–8(f) present the surface SEM micrographs of the surface after the 800 minute immersion in 3.5% NaCl, $pH = 1$ and $pH = 14$, respectively, and in all three cases,

demonstrates no surface morphology degradation compared to the surface image (Figure 8(c) at the same magnification) prior to the long term corrosion tests. Figure 8(g) summarizes the surface composition data obtained from EDX spectra collected at a low magnification of 500X on superhydrophobic samples immersed in the three pH solutions. As seen in the XPS data discussed earlier (section 3.1), the modification agent (stearic acid) comprises carbon and oxygen, whereas the corrosive environment contains chlorine (for NaCl case), sulfur ($pH = 1$), and sodium ($pH = 14$). There is almost no change in carbon, oxygen, and copper content of the surfaces after long term corrosion tests for all three cases, which confirms the surface composition stability along with the morphology stability shown by SEM analysis. Moreover, the absence of Cl, Na, and S in the collected EDS spectra of the test samples after the long term corrosion test implies absence of any residual corrosion footprint on the surface. This is evidence of the outstanding superhydrophobicity and slipperiness of the surface that effectively shields the base metal substrate from the invasive corrosive elements in the solutions. As further evidence of the integrity of the surfaces following long term corrosion, Figure 8(h) presents the contact angle measurements before and after the long term corrosion tests in the three solutions. It is seen that the surfaces remained strongly superhydrophobic with contact angle above 150 degrees in all the cases and, furthermore, no significant change is seen before and after long term corrosion tests in saline, harshly acidic, and harshly alkaline corrosive environments. The results in Figures 7 and 8 sturdily demonstrate the excellent anti-corrosion performance and stability of the electrodeposited superhydrophobic copper surfaces.

3.4. Effect of temperature on corrosion.

It is well known that the corrosion mechanisms are accelerated at the higher temperatures. Most of the studies in the literature have focused on corrosion performance of non-wetting surfaces at lower temperatures. In order to assess the temperature-dependent corrosion characteristics, corrosion measurements were made at a higher temperature of $50°C$ on bare copper and the fabricated superhydrophobic surfaces immersed in the three pH solutions. The corrosion resistance and the corrosion rate, derived as described in section 3.2, are presented for bare copper and superhydrophobic surfaces with varying functionalization time in Figures 9(a) and 9(b), respectively. It is seen that the corrosion resistance drops below that for bare copper for superhydrophobic surfaces functionalized for less than 8 h in the case of immersion in 3.5% NaCl and for less than 24 h in the case of immersion in solutions with $pH = 1$ or $pH = 14$.

Corresponding trends of increase in corrosion rate are noted in Figure 9(b) for the smaller functionalization times. For a functionalization time of 72 h, however, the corrosion resistance and the corrosion rate are about an order of magnitude improved compared to bare copper, in the case of immersion in 3.5% NaCl, and about a factor of 3 better in the case of immersion in extremely acidic or extremely alkaline environments. This suggests that superhydrophobic surfaces with longer functionalization times are warranted for applications to high temperature.

A comparison between the study at 50℃ and room temperature, Figure 9(a) and Figure 3(c) respectively, shows the acidic solution to have the highest change in corrosion resistance. followed by pH~7 (3.5% NaCl solution) and the basic solution. Corrosion is a chemical reaction in nature, where an increase in temperature increases the number of species that have sufficient energy to overcome the corrosion redox reaction activation energy barrier. The main anodic oxidation pathway in the presence of high concentration of the hydronium ion in case of $pH = 1$ is the H^+ reduction reaction rather than oxygen reduction reaction. The higher available energy in the system, because of the higher temperature, and the hydronium reduction pathway both contribute to the increased corrosion rate for the case of $pH = 1$. Unlike oxygen, the concentration of halide anions (Cl^-) does not decrease with increase in the temperature and for the case of pH~7 (3.5% NaCl) the anodic oxidation reaction rate increases, and thus the corrosion rate. For $pH = 14$, the concentration of the hydronium ($or\ H^+$) is insignificant, being 13 and 7 orders of magnitude less compared to $pH = 1$ and 7, respectively, and the corrosion mechanism follows the anodic oxygen reduction pathway. Since less oxygen is soluble at 50℃ compared to room temperature, the corrosion rate increases less intensely compared to the two other cases.

The higher corrosion resistance of bare copper compared to surfaces with functionalization time below 24 hours can be attributed to the readiness of the bare copper surface to corrosion at the OCP resting period before the polarization test begins. This period has given the bare copper sample enough time to develop a relatively passive diffusive film at the vicinity of the surface. On the other hand, it is worth noting that for the calculation of the current densities apparent surface area of the test samples has been considered, which is less than the actual surface area in case of rough superhydrophobic surfaces and identical to actual surface area for case of bare copper.

The influence of corrosion at the higher temperature in the case of a superhydrophobic

surface functionalized for 24 h is examined in Figure 10, in terms of the surface morphology using SEM (Figures 10(a)–(f)), chemical composition using an EDX analysis (Figure 10(g)), and the water contact angle before and after the corrosion test at 50°C (Figure 10(h)). Figures 10(a)–(c) present the morphology of the surface at three different magnifications, prior to the corrosion test, while Figures 10(d)–(f) show the surface morphologies after the corrosion test at in 3.5% NaCl (Figure 10(d)), harshly acidic, $pH = 1$, solution (Figure 10(e)) and harshly alkaline, $pH = 14$, solution (Figure 10(f)). The effect of the increased temperature is to lower the surface tension of the corrosive liquid, causing more contact with the solid surface. This clearly explains the sparse salt particles on the surface after immersion in 3.5% NaCl solution in Figure 10(d) and the presence of sodium peak in the EDX spectrum Figure 10(g). Likewise, the slight deformation of the surface morphology in Figure 10(e), and the presence of sulfur even though in trace quantity in Figure 10(g), is attributed to the same effect after the corrosion test in the harshly acidic aqueous solution of H_2SO_4 with $pH = 1$ at 50°C. Figure 10(f) does not show a detectable morphology change for the case of $pH = 14$ solution except sparse particles. The $pH = 14$ was obtained by hydrolysis of NaOH in DI-water. A significant sodium peak is observed in Figure 10(g) for the case of $pH = 14$ relative to the other two cases. This observation is in agreement with the smaller contact angle measured after immersion in $pH = 14$ compared to the post-immersion contact angles measured for $pH = 1$ and 3.5% NaCl in Figure 10(h). Since the disassociation constant (pKa) of stearic acid is 10.15 [56, 57], the functionalization agent on the surface behaves like an acid in contact with a $pH = 14$ solution and shows basic behavior in contact with $pH = 1$ corrosive solution. Besides, the electrode reduction potential table [58] suggests reactivity of H_2SO_4 and non-reactivity of NaOH with copper. Considering all these factors, besides the high solubility of copper sulfate in water clearly explains the relatively high intensity of the Na peak for the sample immersed in a $pH = 14$ (strongly alkaline) solution, whereas the S concentration in the case of $pH = 1$ (strongly acidic) is relatively small. The residual sodium on the surface after corrosion test for the case of $pH = 14$ is most likely in the form of precipitated NaOH after the sample dried in air, similar to the NaCl crystals distinguishable in the SEM image of 3.5% NaCl in Figure 10(d).

Figure 10(h) presents the change in the water contact angle before and after the high temperature corrosion tests, in the three solutions. In general, Figure 10(h) demonstrates that the superhydrophobic surfaces retain their non-wetting character after corrosion test in 50°C, with

water contact angle of 156.74 ± 2.95 and 152.32 ± 1.23 degrees, respectively, after immersion in saline and extremely acidic ($pH = 1$) solutions. It has been reported in the literature that superhydrophobic surfaces tend to degrade in their water contact angle after immersion in harshly acidic and harshly alkaline solutions at room temperature [35]. In contrast, the superhydrophobic surfaces studied here not only showed almost no change in water contact angle after long term immersion in all the cases at room temperature (Figure 8) but also showed rejuvenated superhydrophobic behavior after corrosion test in 50°C for two cases of saline and acidic corrosive environments, as seen in Figure 10(h). The roll-off angle after long term test at 23°C was measured as 4.0 ± 1.4, 3.0 ± 1.5, and 3.2 ± 0.8 degrees for $pH = 1, pH \sim 7$ (%3.5 NaCl), and $pH = 14$, respectively, which is not a significant change to the value of 3.0 ± 0.5 degrees before the test. Similarly, the roll-off angle after immersion in harsh acidic environment ($pH = 1$) and saline solution ($pH \sim 7$) at 50°C was measured as 8.2 ± 2.6 and 6.8 ± 3.2 degrees, respectively, while pinning was observed for the case of the harshly alkaline solution. The drop in the water contact angle after immersion in the $pH = 14$ solution is attributed to the change in the degree of hydrophobicity due to the sodium contained molecules leftover on the surface.

The discussion so far pertained to one specific high temperature value, and it is of interest to consider the corrosion behavior over a range of temperatures. To this end, considering the case of immersion in 3.5% NaCl of a superhydrophobic surface functionalized for 72 h, the corrosion rate was also measured using PDP method explained in section 2.4 for temperature values of 23°C to 35°C, 50°C, 70°C, and 85°C. A functionalization time of 72 h was selected for this mean based on the functionalization parametric study. For statistical significance, the tests were repeated three times at each temperature. Figure 11 presents the variation of the corrosion rate with the inverse of the absolute temperature (in Kelvin) on a semi-log plot. The decrease in the standard deviation of measured corrosion rate values at higher temperatures is attributed to the increase in homogeneity of the porous rough superhydrophobic surfaces. Corrosion is a surface phenomenon that begins at surface defects, as the temperature increases the randomly formed needle-like modification agent atop the multiscale electrodeposited layer tend to soften to a less rough and more homogenous structure. The linear nature of the variation in the semi-log plot suggests an Arrhenius relationship between the corrosion rate and the temperature, where the slope is the activation energy in the exponential term and the intercept on the ordinate is the pre-exponential factor. Based on a least-squares linear regression fit through the data, the following

equation is derived for the temperature-dependent corrosion rate of the superhydrophobic surface in 3.5% NaCl solution.

$$\mathrm{CR} = 4.227 \times 10^{11} \cdot \exp\left(-\frac{9797.18}{T}\right)$$

The Arrhenius equation serves to investigate corrosion of the superhydrophobic surfaces presented in this article in saline environment at any temperature of interest in the range of 23–85°C. Note that the Arrhenius relationship is developed here for a functionalization time of 72 h and 3.5% NaCl, based on the result in Figure 9 that showed this functionalization time to yield the greatest corrosion inhibition for the entire range of pH values. A similar relationship may be derived for other functionalization times and other pH values following the methodology presented.

3.5. Chemical stability over a wide range of pH and salinity.

The results so far in this section demonstrated the excellent corrosion inhibition performance of the superhydrophobic surfaces in two extreme values of pH namely, the strongly acidic ($pH = 1$) and the strongly basic ($pH = 14$). It was seen that hydrophobicity is the major contributor to the corrosion inhibition effect. To demonstrate the durability of the superhydrophobic surface in corrosive environments the contact angle of aqueous solutions with various pH values ranging continuously from $pH = 1$ to $pH = 14$ was studied, as shown in Figure 12(a). The highest contact angle value was recorded as 161.35 ± 1.58 degrees for $pH = 7$ and an average contact angle over 158 degrees was observed for all the other pH values. The lowest contact angle of 153.38 ± 3.15 degrees was measured for $pH = 14$. Moreover, the roll-off angles for pH values between 2 and 12 were recorded to be less than 5 degrees and less than 10 degrees for $pH = 1$ and 12, respectively, and were measured as 15.8 ± 3.5 and 22.0 ± 4.7 degrees for $pH = 13$ and 14, respectively. The variation in contact angle in Figure 12(a) is well aligned with the corrosion performance studied in various pH solutions, where superhydrophobic surfaces had the least corrosion resistance in the extremely alkaline ($pH = 14$) solution compared to immersion in the 3.5% NaCl and the extremely acidic ($pH = 1$) solutions. The corrosion studies reported in this section considered a simulated marine environment with a salinity of 3.5% NaCl, which corresponds to 0.6 M sodium chloride. The hydrophobicity of the surface exposed to various ionic strength of the aqueous halide solutions was also investigated, as summarized in Figure

12(b). The water contact angle variation with the ionic strength clearly demonstrates the stability of the superhydrophobic surfaces in solutions with high ionic strength. In all the cases, the halide solution droplet showed an average contact angle of 158 degrees or higher, with contact angles as high as 161.3 degrees and average roll-off angle of 5.8 ± 1.2 degrees. The contact angle and roll-off angle values reported in this section are summarized in Table 4.

The corrosion inhibition mechanism was discussed to be divided into three major mechanisms: I) physical barrier effect of the coating, II) the repulsion force due to excessive charge at the water/SHS interface, and III) air cushion due to heterogeneous wetting regime of the SHS. Based on EIS analysis, detailed in section 3.2, the first mechanism is not significant compared to the others since $Q_f < Q_{dl}$ and $R_f < R_{ct}$. Furthermore, the insignificant change in contact angle values with increasing the ionic strength, Figure 12(b), indicates that the second mechanism should not be the major contributor as well. As a result, it was surmised that hydrophobicity is the major contributor to the corrosion inhibition effect.

The results in this section collectively offer evidence of the robustness of the superhydrophobic surfaces fabricated by the electrodeposition method in a wide range of corrosive environments in practice. While the focus of this paper was on superhydrophobic surfaces, a companion class of liquid infused surfaces also offer non-wetting properties. Corrosion characteristics of liquid infused porous surfaces will be considered in a future work in comparison the results presented in this article. Furthermore, the corrosion durability of the non-wetting surfaces subject to abrasive and other harsh mechanical environments are also of significance in the design of the surfaces in practice, and will be considered in a future study.

4. CONCLUSIONS

A facile method was presented for the fabrication of multiscale textured surfaces on copper via electrodeposition. The fabrication time was less than five minutes and with low power consumption in comparison to similar methods presented in the literature. The fabricated surfaces, functionalized with an environmentally benign stearic acid, demonstrated water contact angle over 155 degrees, roll-off angle below 3 degrees, and contact angle hysteresis below 5 degrees. The fabricated superhydrophobic surfaces were systematically studied for their corrosion inhibition performance in a range of corrosive environments from the extremely acidic ($pH = 1$) to saline 3.5% NaCl solution to mimic the marine environment, and an extremely

alkaline ($pH = 14$) environment. The corrosion inhibition was shown to increase with increase in functionalization time, and corrosion inhibition efficiency of over 99% was demonstrated at room temperature in all the harsh corrosion environments studied. The superhydrophobic surfaces were shown to inhibit corrosion by two to four orders of magnitude compared to bare copper. Long-term immersion studies demonstrated the excellent stability of the surfaces in all corrosive environments, and corrosion at higher temperatures suggested the need for a longer duration functionalization for application of the superhydrophobic surfaces to elevated temperature environments. An Arrhenius relationship was developed for the temperature-dependent corrosion rate of the superhydrophobic surface in 3.5% NaCl solution. Overall, the superhydrophobicity of the surface was found to be a major contributing factor to the corrosion resistance, and the superhydrophobicity was shown to be robust in a range of pH and ionic strength of aqueous halide solutions.

ACKNOWLEDGMENT AND DISCLAIMER

The material reported in this publication is based upon work supported by the U.S. Department of Energy under Award Number DE-FE0031556. This publication was prepared as an account of work sponsored by an agency of the United States Government. Neither the United States Government nor any agency thereof, nor any of their employees, makes any warranty, express or implied, or assumes any legal liability or responsibility for the accuracy, completeness, or usefulness of any information, apparatus, product, or process disclosed, or represents that its use would not infringe on privately owned rights. Reference herein to any specific commercial product, process, or service by trade name, trademark, manufacturer, or otherwise does not necessarily constitute or imply its endorsement, recommendation, or favoring by the United States Government or any agency thereof. The views and opinions of the authors expressed herein do not necessarily state or reflect those of the United States Government or any agency thereof.

DATA AVAILABILITY

The raw data required to reproduce these findings are already included in the presented figures. The processed data required to reproduce these findings are included in the presented figures.

REFERENCES

[1] E.-S.M. Sherif, Effects of 2-amino-5-(ethylthio)-1, 3, 4-thiadiazole on copper corrosion as a corrosion inhibitor in 3% NaCl solutions, Applied surface science, 252 (2006) 8615-8623.

[2] D.-Q. Zhang, L.-X. Gao, G.-D. Zhou, Inhibition of copper corrosion in aerated hydrochloric acid solution by heterocyclic compounds containing a mercapto group, Corrosion science, 46 (2004) 3031-3040.

[3] E. Abelev, D. Starosvetsky, Y. Ein-Eli, Enhanced copper surface protection in aqueous solutions containing short-chain alkanoic acid potassium salts, Langmuir, 23 (2007) 11281-11288.

[4] Y. Qiang, S. Fu, S. Zhang, S. Chen, X. Zou, Designing and fabricating of single and double alkyl-chain indazole derivatives self-assembled monolayer for corrosion inhibition of copper, Corrosion Science, 140 (2018) 111-121.

[5] R.N. Wenzel, Resistance of solid surfaces to wetting by water, Industrial Engineering Chemistry, 28 (1936) 988-994.

[6] A. Cassie, S. Baxter, Wettability of porous surfaces, Transactions of the Faraday society, 40 (1944) 546-551.

[7] D.L. Hu, B. Chan, J.W. Bush, The hydrodynamics of water strider locomotion, Nature, 424 (2003) 663.

[8] Z. Sun, T. Liao, K. Liu, L. Jiang, J.H. Kim, S.X. Dou, Fly-Eye Inspired Superhydrophobic Anti-Fogging Inorganic Nanostructures, Small, 10 (2014) 3001-3006.

[9] S. Wang, Z. Yang, G. Gong, J. Wang, J. Wu, S. Yang, L.J. Jiang, Icephobicity of penguins spheniscus humboldti and an artificial replica of penguin feather with air-infused hierarchical rough structures, The Journal of Physical Chemistry C, 120 (2016) 15923-15929.

[10] J. Ju, H. Bai, Y. Zheng, T. Zhao, R. Fang, L. Jiang, A multi-structural and multi-functional integrated fog collection system in cactus, Nature communications, 3 (2012) 1247.

[11] J. Genzer, K.J.S. Efimenko, Creating long-lived superhydrophobic polymer surfaces through mechanically assembled monolayers, 290 (2000) 2130-2133.

[12] T. Nishino, M. Meguro, K. Nakamae, M. Matsushita, Y. Ueda, The lowest surface free energy based on– CF3 alignment, Langmuir, 15 (1999) 4321-4323.

[13] S. Khodakarami, H. Zhao, K.F. Rabbi, N. Miljkovic, Scalable Corrosion-Resistant Coatings for Thermal Applications, ACS Applied Materials & Interfaces, 13 (2021) 4519-4534.

[14] Y. Fan, C. Li, Z. Chen, H. Chen, Study on fabrication of the superhydrophobic sol–gel films based on copper wafer and its anti-corrosive properties, Applied Surface Science, 258 (2012) 6531-6536.

[15] A.V. Rao, S.S. Latthe, S.A. Mahadik, C. Kappenstein, Mechanically stable and corrosion resistant superhydrophobic sol–gel coatings on copper substrate, Applied Surface Science, 257 (2011) 5772-5776.

[16] G. Jiang, L. Luo, L. Tan, J. Wang, S. Zhang, F. Zhang, J. Jin, Microsphere-Fiber Interpenetrated Superhydrophobic PVDF Microporous Membranes with Improved Waterproof and Breathable Performance, ACS applied materials interfaces, 10 (2018) 28210-28218.

[17] K.A. Emelyanenko, N.A. Sanzharovsky, E.V. Chulkova, A.A. Ganne, A.M. Emelyanenko, L.B. Boinovich, Superhydrophobic corrosion resistant coatings for copper via IR nanosecond laser processing, Materials Research Express, 5 (2018) 115001.

[18] Y. Wan, M. Chen, W. Liu, X. Shen, Y. Min, Q. Xu, The research on preparation of superhydrophobic surfaces of pure copper by hydrothermal method and its corrosion resistance, Electrochimica Acta, 270 (2018) 310-318.
[19] B. Zhang, W. Xu, Q. Zhu, Y. Sun, Y. Li, Mechanically robust superhydrophobic porous anodized AA5083 for marine corrosion protection, Corrosion Science, 158 (2019) 108083.
[20] N. Lin, L. Zhang, J. Zou, Q. Liu, S. Yuan, L. Zhao, Y. Yu, Z. Liu, Q. Zeng, X. Liu, A combined surface treatment of surface texturing-double glow plasma surface titanizing on AISI 316 stainless steel to combat surface damage: Comparative appraisals of corrosion resistance and wear resistance, Applied Surface Science, 493 (2019) 747-765.
[21] C. Scheuer, F. Possoli, P. Borges, R. Cardoso, S. Brunatto, AISI 420 martensitic stainless steel corrosion resistance enhancement by low-temperature plasma carburizing, Electrochimica Acta, 317 (2019) 70-82.
[22] E. Berretti, N. Calisi, A. Capaccioli, L. Capozzoli, A. Hamouda, A. Giaccherini, W. Giurlani, A. Ienco, S. Martinuzzi, M. Innocenti, Electrodeposited white bronzes on brass: Corrosion in 3.5% sodium chloride solution, Corrosion Science, 175 (2020) 108898.
[23] R. Tang, G.R. Joshi, H. Zhao, S.P. Venkateswaran, P.J. Withers, P. Xiao, The influence of electrodeposited Ni-Co alloy coating microstructure on CO2 corrosion resistance on X65 steel, Corrosion Science, 167 (2020) 108485.
[24] C.-X. Wang, X.-F. Zhang, A non-particle and fluorine-free superhydrophobic surface based on one-step electrodeposition of dodecyltrimethoxysilane on mild steel for corrosion protection, Corrosion Science, 163 (2020) 108284.
[25] J. Ou, W. Hu, M. Xue, F. Wang, W. Li, Superhydrophobic surfaces on light alloy substrates fabricated by a versatile process and their corrosion protection, ACS applied materials & interfaces, 5 (2013) 3101-3107.
[26] J.-P. Lee, S. Choi, S. Park, Extremely superhydrophobic surfaces with micro-and nanostructures fabricated by copper catalytic etching, Langmuir, 27 (2010) 809-814.
[27] B. Qian, Z. Shen, Fabrication of superhydrophobic surfaces by dislocation-selective chemical etching on aluminum, copper, and zinc substrates, Langmuir, 21 (2005) 9007-9009.
[28] T. Darmanin, E.T. de Givenchy, S. Amigoni, F. Guittard, Superhydrophobic surfaces by electrochemical processes, Advanced materials, 25 (2013) 1378-1394.
[29] G. He, S. Lu, W. Xu, S. Szunerits, R. Boukherroub, H. Zhang, Controllable growth of durable superhydrophobic coatings on a copper substrate via electrodeposition, Physical Chemistry Chemical Physics, 17 (2015) 10871-10880.
[30] F. Su, K. Yao, C. Liu, P. Huang, Rapid fabrication of corrosion resistant and superhydrophobic cobalt coating by a one-step electrodeposition, Journal of The Electrochemical Society, 160 (2013) D593-D599.
[31] F. Su, K. Yao, Facile fabrication of superhydrophobic surface with excellent mechanical abrasion and corrosion resistance on copper substrate by a novel method, ACS applied materials interfaces, 6 (2014) 8762-8770.
[32] A. Haghdoost, R. Pitchumani, Fabricating superhydrophobic surfaces via a two-step electrodeposition technique, Langmuir, 30 (2013) 4183-4191.
[33] J. Liu, X. Fang, C. Zhu, X. Xing, G. Cui, Z. Li, Fabrication of superhydrophobic coatings for corrosion protection by electrodeposition: A comprehensive review, Colloids and Surfaces A: Physicochemical and Engineering Aspects, 607 (2020) 125498.
[34] E. Vazirinasab, R. Jafari, G. Momen, Application of superhydrophobic coatings as a

corrosion barrier: A review, Surface and Coatings Technology, 341 (2018) 40-56.
[35] Y. Liu, S. Li, J. Zhang, Y. Wang, Z. Han, L. Ren, Fabrication of biomimetic superhydrophobic surface with controlled adhesion by electrodeposition, Chemical Engineering Journal, 248 (2014) 440-447.
[36] L. Liu, R. Chen, W. Liu, Y. Zhang, X. Shi, Q. Pan, Fabrication of superhydrophobic copper sulfide film for corrosion protection of copper, Surface Coatings Technology, 272 (2015) 221-228.
[37] P. Wang, R. Qiu, D. Zhang, Z. Lin, B. Hou, Fabricated super-hydrophobic film with potentiostatic electrolysis method on copper for corrosion protection, Electrochimica Acta, 56 (2010) 517-522.
[38] P. Wang, D. Zhang, R. Qiu, J. Wu, Super-hydrophobic metal-complex film fabricated electrochemically on copper as a barrier to corrosive medium, Corrosion Science, 83 (2014) 317-326.
[39] Y. Liu, S. Li, J. Zhang, J. Liu, Z. Han, L. Ren, Corrosion inhibition of biomimetic super-hydrophobic electrodeposition coatings on copper substrate, Corrosion Science, 94 (2015) 190-196.
[40] ASTM G3-14(2019), Standard Practice for Conventions Applicable to Electrochemical Measurements in Corrosion Testing, ASTM International, West Conshohocken, PA, 2019..
[41] N.T. Kirkland, N. Birbilis, M. Staiger, Assessing the corrosion of biodegradable magnesium implants: a critical review of current methodologies and their limitations, Acta biomaterialia, 8 (2012) 925-936.
[42] M.C. Biesinger, Advanced analysis of copper X-ray photoelectron spectra, Surface and Interface Analysis, 49 (2017) 1325-1334.
[43] M. Stern, A.L. Geary, Electrochemical polarization I. A theoretical analysis of the shape of polarization curves, Journal of the electrochemical society, 104 (1957) 56-63.
[44] F. Su, K. Yao, C. Liu, P. Huang, Rapid fabrication of corrosion resistant and superhydrophobic cobalt coating by a one-step electrodeposition, Journal of the Electrochemical Society, 160 (2013) D593.
[45] N. Xu, D.K. Sarkar, X.G. Chen, H. Zhang, W. Tong, Superhydrophobic copper stearate/copper oxide thin films by a simple one-step electrochemical process and their corrosion resistance properties, RSC advances, 6 (2016) 35466-35478.
[46] S. Cruz-Manzo, Kramers-Kronig (K-K) Analysis in ZView Software for Evaluation of EIS Measurements in Polymer Electrolyte Fuel Cells, https://dx.doi.org/10.13140/RG.2.1.1094.0887/1 (Accessed February 2021).
[47] D.Q. Zhang, P.-H. Liu, L.X. Gao, H.G. Joo, K.Y. Lee, Photosensitive self-assembled membrane of cysteine against copper corrosion, Materials Letters, 65 (2011) 1636-1638.
[48] F. Growcock, R. Jasinski, Time-Resolved Impedance Spectroscopy of Mild Steel in Concentrated Hydrochloric Acid, Journal of the Electrochemical Society, 136 (1989) 2310-2314.
[49] B. Hirschorn, M.E. Orazem, B. Tribollet, V. Vivier, I. Frateur, M. Musiani, Determination of effective capacitance and film thickness from constant-phase-element parameters, Electrochimica Acta, 55 (2010) 6218-6227.
[50] J.O.M. Bockris, A.K. Reddy, Modern electrochemistry 2B: electrodics in chemistry, engineering, biology and environmental science, Springer Science & Business Media, 2000.
[51] L.B. Boinovich, A.M. Emelyanenko, A.D. Modestov, A.G. Domantovsky, K.A.

Emelyanenko, Not simply repel water: the diversified nature of corrosion protection by superhydrophobic coatings, Mendeleev Communications, 27 (2017) 254-256.
[52] L. Boinovich, A. Emelyanenko, A. Modestov, A. Domantovsky, A. Shiryaev, K. Emelyanenko, O. Dvoretskaya, A. Ganne, Corrosion behavior of superhydrophobic aluminum alloy in concentrated potassium halide solutions: When the specific anion effect is manifested, Corrosion Science, 112 (2016) 517-527.
[53] C. Tian, Y. Shen, Structure and charging of hydrophobic material/water interfaces studied by phase-sensitive sum-frequency vibrational spectroscopy, Proceedings of the National Academy of Sciences, 106 (2009) 15148-15153.
[54] P. Creux, J. Lachaise, A. Graciaa, J.K. Beattie, A.M. Djerdjev, Strong specific hydroxide ion binding at the pristine oil/water and air/water interfaces, The Journal of Physical Chemistry B, 113 (2009) 14146-14150.
[55] R. Zimmermann, U. Freudenberg, R. Schweiß, D. Küttner, C. Werner, Hydroxide and hydronium ion adsorption—A survey, Current Opinion in Colloid Interface Science, 15 (2010) 196-202.
[56] K. Quast, The use of zeta potential to investigate the pKa of saturated fatty acids, Advanced Powder Technology, 27 (2016) 207-214.
[57] J.R. Kanicky, D.O. Shah, Effect of degree, type, and position of unsaturation on the pKa of long-chain fatty acids, Journal of colloid interface science, 256 (2002) 201-207.
[58] A.J. Bard, L.R. Faulkner, J. Leddy, C.G. Zoski, Electrochemical methods: fundamentals and applications, Wiley New York, 1980.

Table 1: Corrosion parameters from the potentiodynamic polarization tests in solutions of different pH values at 23°C

Samples	3.5% NaCl (pH ≈ 7)					pH = 1					pH = 14				
	β_{an}	β_{cat}	j_{corr}	E_{corr}	η	β_{an}	β_{cat}	j_{corr}	E_{corr}	η	β_{an}	β_{cat}	j_{corr}	E_{corr}	η
Bare Cu	66.38	107.05	6.55	-0.229	–	71.31	214.98	30.4	-0.008	–	48.94	276.92	350	-0.245	–
t_f = 1 h	47.15	153.03	1.97	-0.154	69.99	31.39	85.312	12.9	0.030	54.04	46.09	266.46	444	-0.255	26.14
t_f = 2 h	56.89	135.33	1.02	-0.191	84.50	38.41	715.81	3.60	0.010	79.67	44.26	298.05	304	-0.258	34.74
t_f = 4 h	60.88	127.53	0.79	-0.198	88.00	43.04	275.00	1.94	0.002	84.75	48.89	260.46	116	-0.246	71.30
t_f = 8 h	69.38	226.68	0.56	-0.211	91.41	16.83	20.671	1.13	0.032	99.63	50.504	251.27	77.7	-0.259	90.60
t_f = 24 h	67.85	162.77	0.16	-0.213	97.50	38.68	550.00	0.05	0.025	99.12	46.90	277.82	7.59	-0.260	99.46
t_f = 72 h	73.7	157.07	0.02	-0.219	99.78	45.79	371.72	0.006	0.003	99.97	33.05	155.61	1.34	-0.253	99.99

Units: β_{an} and β_{cat} [mV/dec.]; j_{corr} [μA/cm^2]; E_{corr} vs. Ag/AgCl [V]; η [%]

Table 2: Equivalent circuit model parameters for corrosion tests in a 3.5% NaCl solution at 23°C

Samples	R_s	CPE_f		R_f	CPE_{dl}		R_{ct}
		Q_f	n_f		Q_{dl}	n_{dl}	
Bare Cu	2.4	14.36	0.938	0.02	167.07	0.461	2.86
t_f = 1 h	5.6	1.04	0.852	0.90	23.70	0.566	13.61
t_f = 2 h	10.6	4.21	0.806	0.98	9.59	0.302	21.53
t_f = 4 h	10.6	1.62	0.778	1.07	13.30	0.507	60.48
t_f = 8 h	10.6	0.24	0.893	1.10	3.75	0.558	58.14
t_f = 24 h	10.6	0.11	0.897	1.42	2.42	0.518	244.09
t_f = 72 h	10.6	0.02	0.975	3.62	2.75	0.439	1502.60

Units: R_s [Ω ·cm^2]; R_f and R_{ct} [kΩ ·cm^2]; Q [μΩ^{-1}s^{n}cm^{-2}]; n [dimensionless]

Table 3: Equivalent circuit model parameters for corrosion tests in solutions of pH = 1 and pH = 14 values at 23°C

Samples	pH = 1							pH = 14						
	R_s	CPE_f		R_f	CPE_{dl}		R_{ct}	R_s	CPE_f		R_f	CPE_{dl}		R_{ct}
		Q_f	n_f		Q_{dl}	n_{dl}			Q_f	n_f		Q_{dl}	n_{dl}	
Bare Cu	3.10	42.75	0.844	0.9	711.81	0.55	0.4	1.08	678.54	0.510	0.02	3211.10	0.626	0.03
t_f = 1 h	3.13	87.49	0.689	0.80	6032.30	0.442	2.8	1.10	1850.00	0.522	0.01	5118.90	0.651	0.04
t_f = 2 h	3.13	13.88	0.781	5.94	854.64	0.368	14.0	1.16	148.39	0.689	0.01	3870.10	0.529	0.08
t_f = 4 h	3.13	5.47	0.638	4.91	456.97	0.397	61.1	1.10	238.54	0.491	0.01	786.620	0.661	0.24
t_f = 8 h	3.13	0.27	0.770	2.50	4.43	0.493	69.5	1.57	20.38	0.688	0.11	515.93	0.534	0.57
t_f = 24 h	3.13	0.02	0.833	55.86	0.48	0.562	615.0	1.57	1.38	0.677	2.09	23.04	0.587	56.9
t_f = 72 h	3.13	0.01	0.951	540.00	0.40	0.587	1930.0	1.57	0.006	0.867	24.1	1.37	0.453	135.0

Units: R_s [$\Omega \cdot cm^2$]; R_f and R_{ct} [$k\Omega \cdot cm^2$]; Q [$\mu\Omega^{-1}s^n cm^{-2}$]; n [dimensionless]

Table 4: Contact angle and roll-off angle of different various pH and saline solutions on superhydrophobic copper, t_f = 72 h at 23°C

Acidity	Contact angle	Roll-off angle	Basicity	Contact angle	Roll-off angle	Salinity	Contact angle	Roll-off angle
$pH = 1$	158.6±1.2	7.0±3.8	$pH = 8$	160.3±1.1	4.3±1.8	1 M	160.8±1.5	6.4±3.5
$pH = 2$	159.5±1.9	3.2±1.6	$pH = 9$	160.5±2.3	3.0±0.9	1 M	158.9±3.9	7.4±3.9
$pH = 3$	161.6±1.3	3.2±0.8	$pH = 10$	159.7±1.9	4.0±1.3	3 M	158.2±1.7	4.8±2.3
$pH = 4$	160.7±1.8	3.0±1.1	$pH = 11$	160.1±1.8	4.2±1.9	4 M	161.4±3.9	5.7±4.8
$pH = 5$	160.8±0.9	3.0±1.0	$pH = 12$	160.9±2.7	6.2±1.5	5 M	161.3±2.6	4.5±3.9
$pH = 6$	161.4±1.6	2.4±0.5	$pH = 13$	160.1±1.5	15.8±3.5			
$pH = 7$	159.6±1.3	3.3±1.6	$pH = 14$	153.4±3.2	22.0±4.7			

Units: Contact Angle [degree]; Roll-off angle: [degree]

FIGURE CAPTIONS

Figure 1. Schematic of the electrodeposition setup for fabrication of superhydrophobic surfaces.

Figure 2. (a-d) SEMs of surfaces fabricated via electrodeposition at different voltages showing progressively increasing multiscale features and corresponding hydrophobicity or superhydrophobicity; (e) XPS survey spectra and (f) XPS high resolution spectra of superhydrophobic copper surface fabricated via electrodeposition at -1.1 V and functionalized for 24 h in stearic acid.

Figure 3. (a) Tafel plots from corrosion potentiodynamic polarization (PDP) test in 3.5% NaCl (pH ~ 7) solution at 23°C. Variation of corrosion parameters—(b) corrosion current, j_{corr}, and corrosion potential, E_{corr}, (c) corrosion resistance, R_{corr}, and (d) corrosion rate, CR—with functionalization time, t_f, for superhydrophobic copper surfaces at 23°C at different pH solutions.

Figure 4. EIS data curves showing the effects of functionalizing time at 23°C in 3.5% NaCl ($pH{\sim}7$) solution: Nyquist plots of (a) bare copper as reference, and (b) superhydrophobic surfaces (SHS); (c) Bode plots of bare copper control sample and SHS, and (d) Phase diagrams of bare copper control sample and SHS.

Figure 5. EIS data curves showing the effect of pH solution at 23°C: Nyquist plots of (a) bare copper as reference and (b) superhydrophobic surfaces (SHS); (c) Bode plots of bare copper control sample and SHS; (d) Phase diagrams of bare copper control sample and SHS.

Figure 6. Schematic of the equivalent circuit model of EIS data for (a) bare copper control sample and (b) superhydrophobic surfaces; (c) variation of the charge transfer resistance, R_{ct}, derived from the equivalent circuit model for bare copper control sample and superhydrophobic surfaces with functionalization time, t_f, in three different pH solutions.

Figure 7. Variation of (a) corrosion resistance, R_{corr}, and (b) corrosion rate, CR, with immersion time, t_i, for bare copper control sample and superhydrophobic surfaces in three different pH of the immersion solution at T_i = 23℃.

Figure 8. SEM images of superhydrophobic surface (SHS) at three different magnifications, (a–c) before the long term corrosion test and after long term corrosion test in (d)

3.5% NaCl (pH~7), (e) $pH = 1$ and (f) $pH = 14$ aqueous solutions; (g) summary of surface relative atomic percentage of detected elements and (h) contact angle of 10µl DI-water droplet on the surfaces before and after long term corrosion test in different pH solutions at temperature T_i = 23℃.

Figure 9. Variation of (a) corrosion resistance, R_{corr} and (b) corrosion rate, CR, for bare copper control sample and superhydrophobic surfaces showing the effect of immersion time, t_i , and pH of the immersion solution at T_i = 50℃.

Figure 10. SEM images of superhydrophobic surface (SHS) at three different magnifications, (a–c) before the long term corrosion test and after long term corrosion test in (d) 3.5% NaCl (pH~7), (e) $pH = 1$ and (f) $pH = 14$ aqueous solutions; (g) summary of surface relative atomic percentage of detected elements and (h) contact angle of 10µl DI-water droplet on the surfaces before and after long term corrosion test in different pH solutions at temperature T_i = 50℃.

Figure 11. Arrhenius plot of the natural logarithm of the corrosion rate in terms of the reciprocal of absolute temperature for electrodeposited superhydrophobic samples, t_f = 72 h, in 3.5% NaCl aqueous solution.

Figure 12. Effect of (a) pH and (b) ionic strength (salinity) on the droplet contact angle for electrodeposited samples, t_f = 72 h, at room temperature. Note a 3.5% NaCl aqueous solution corresponds to 0.6 M.

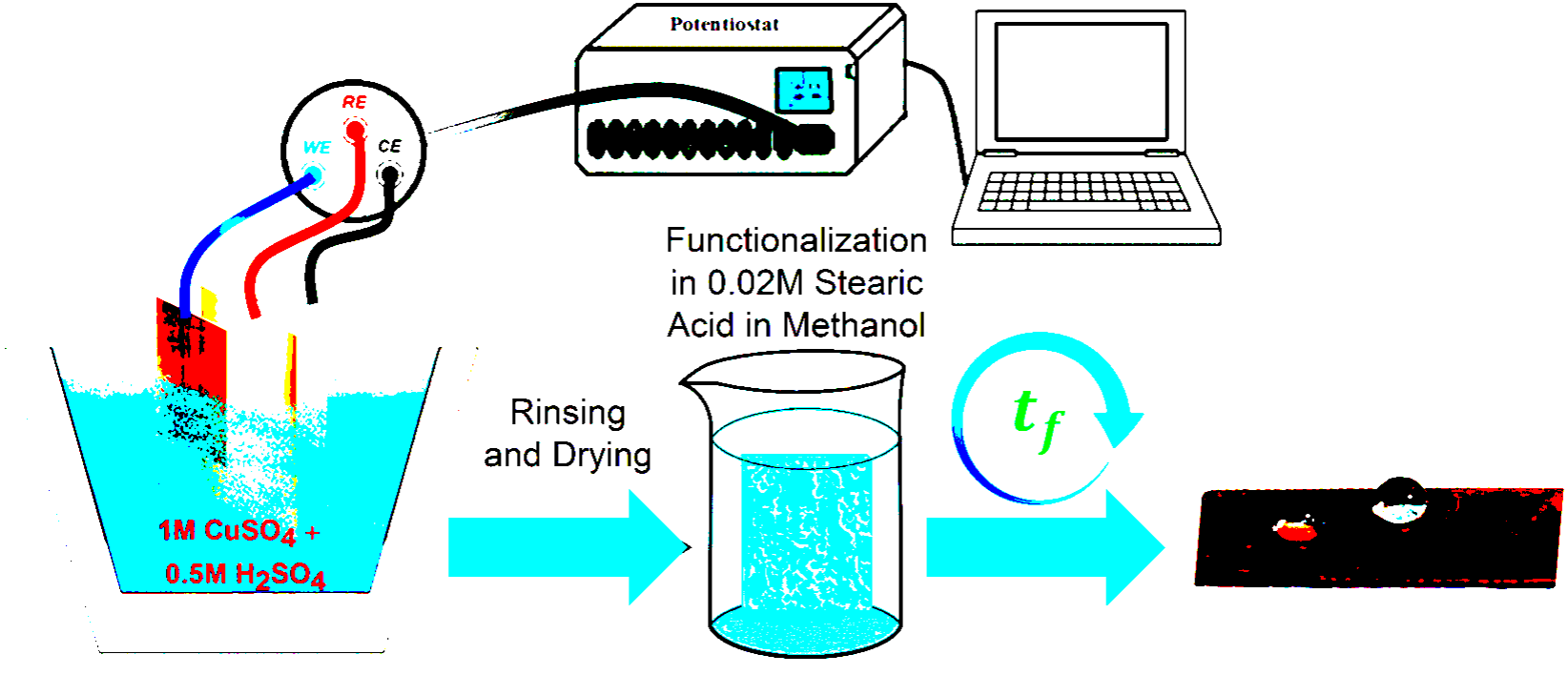

Figure 1: Mousavi and Pitchumani

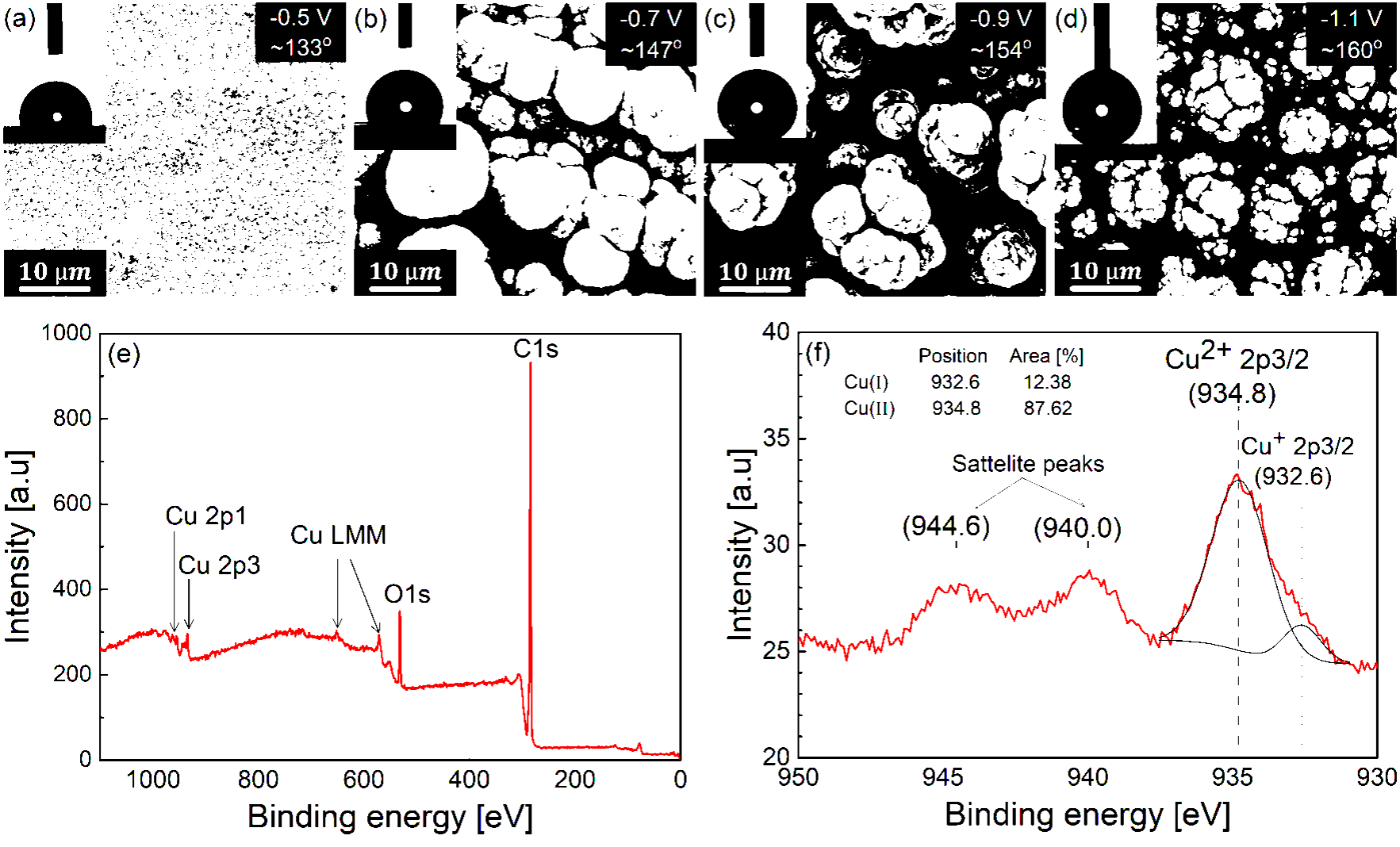

Figure 2: Mousavi and Pitchumani

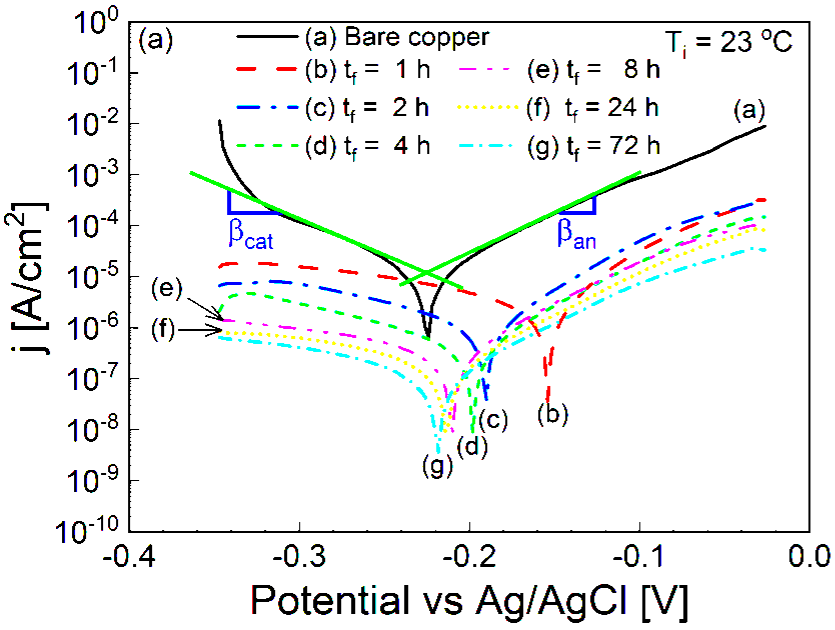

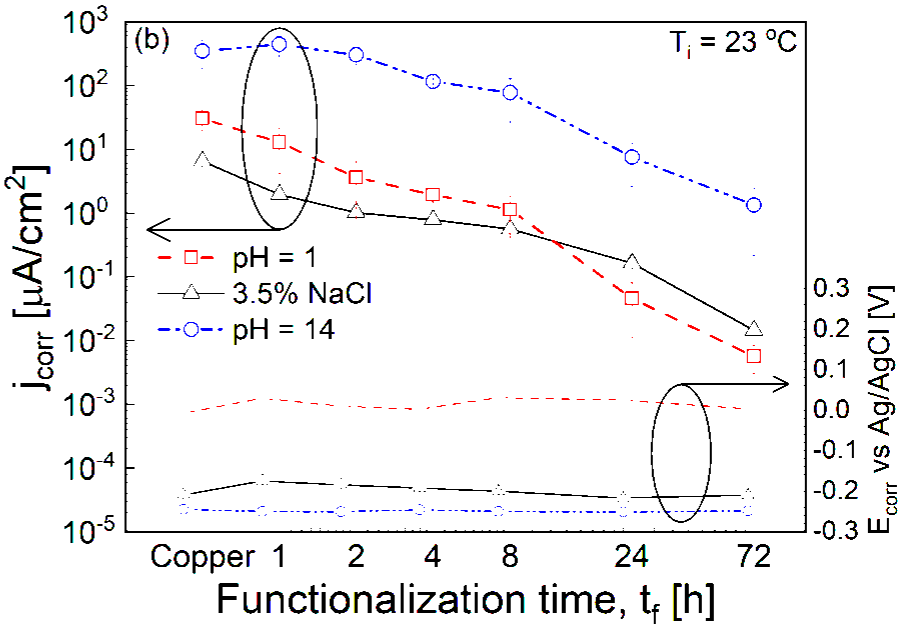

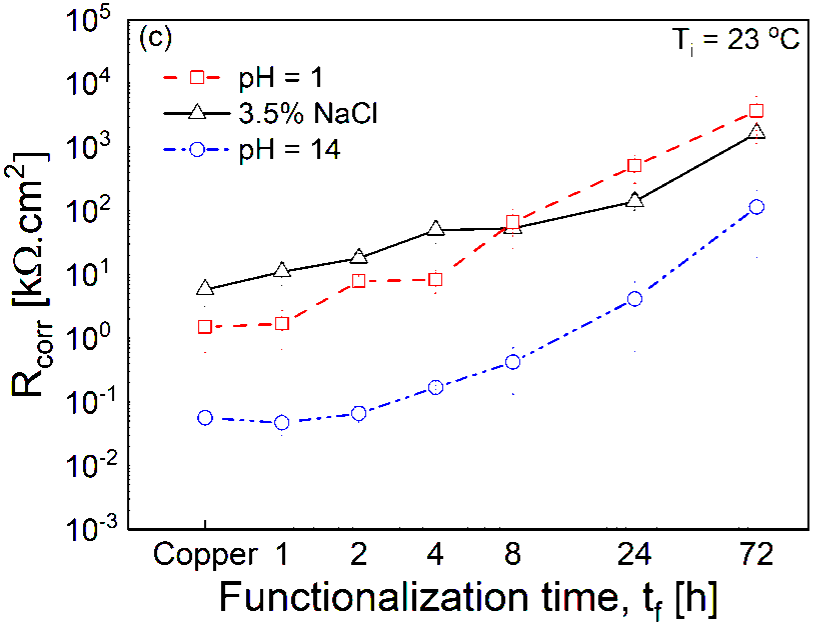

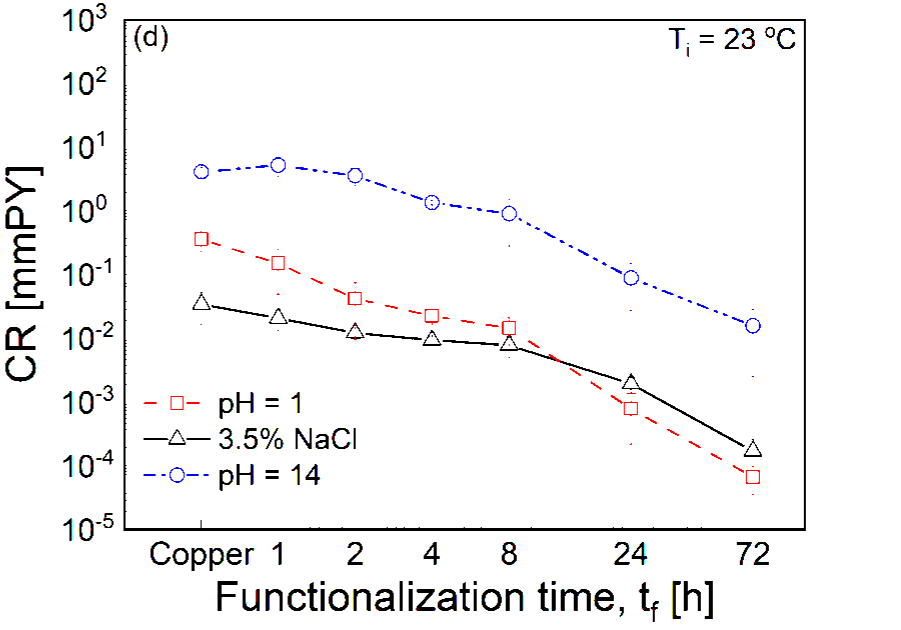

Figure 3: Mousavi and Pitchumani

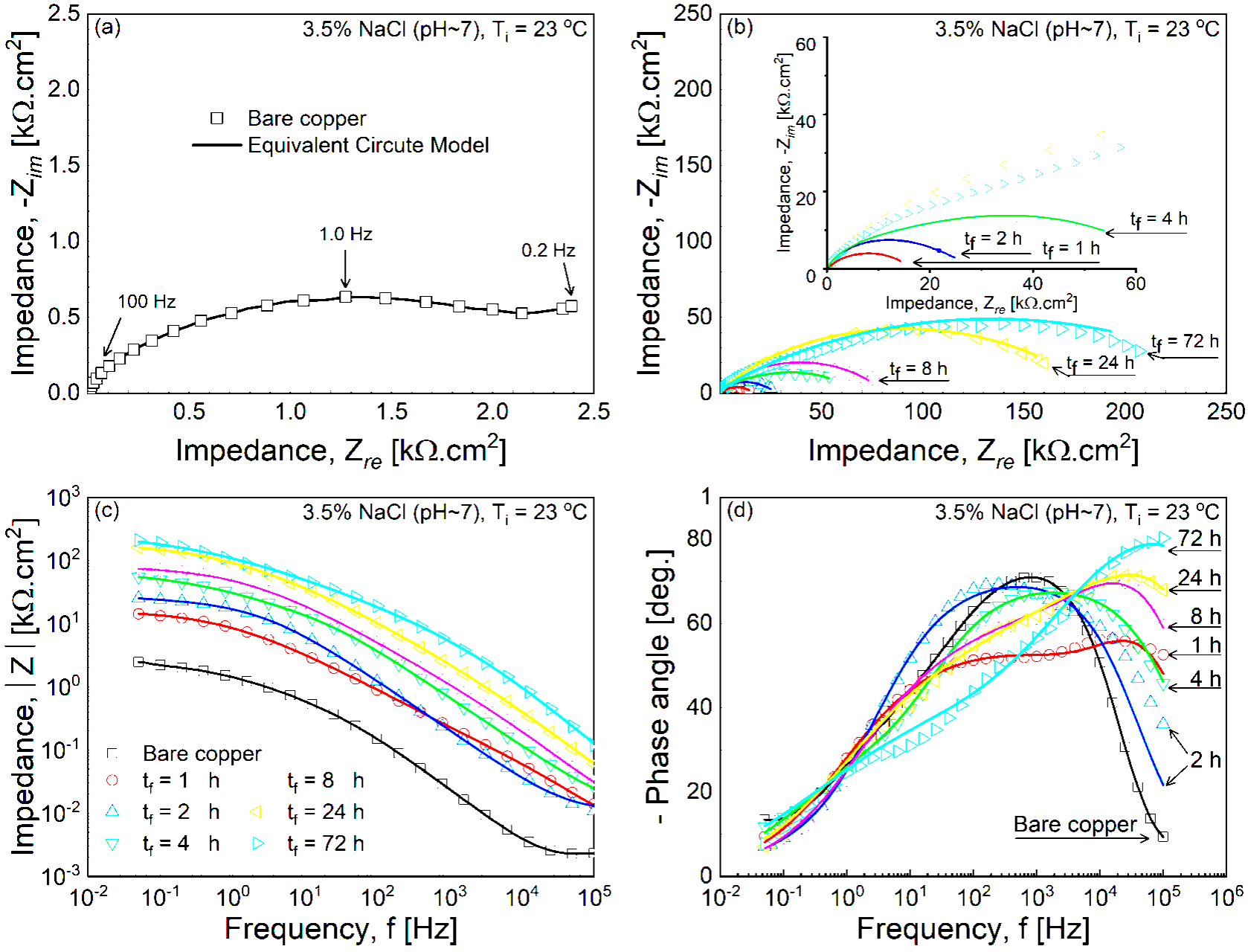

Figure 4: Mousavi and Pitchumani

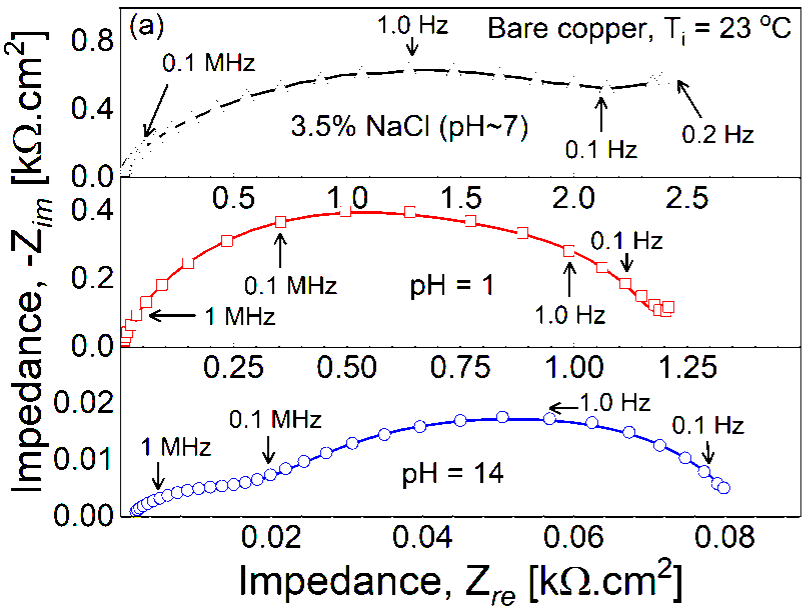

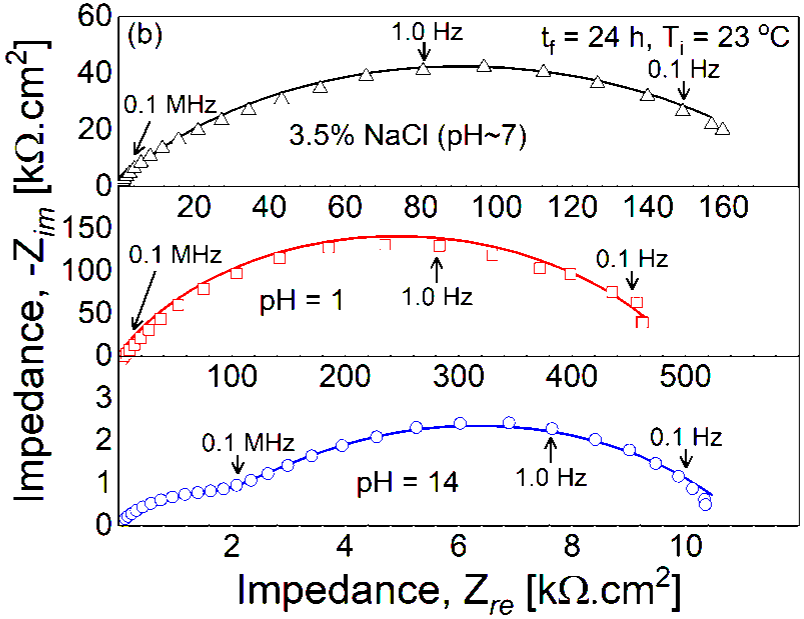

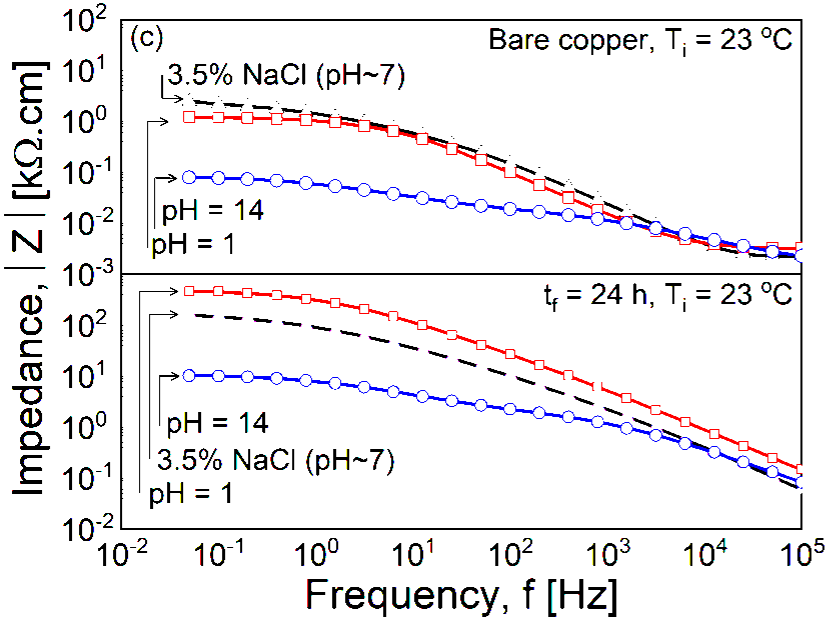

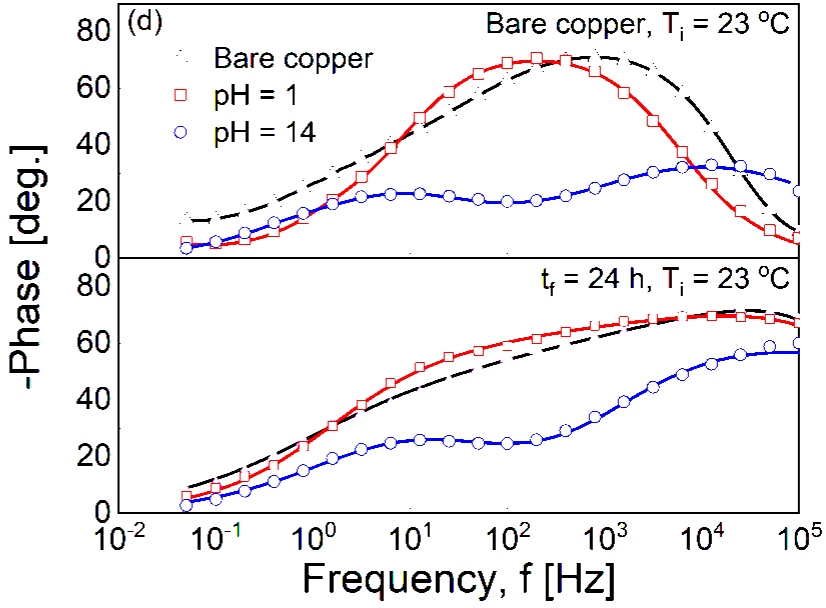

Figure 5: Mousavi and Pitchumani

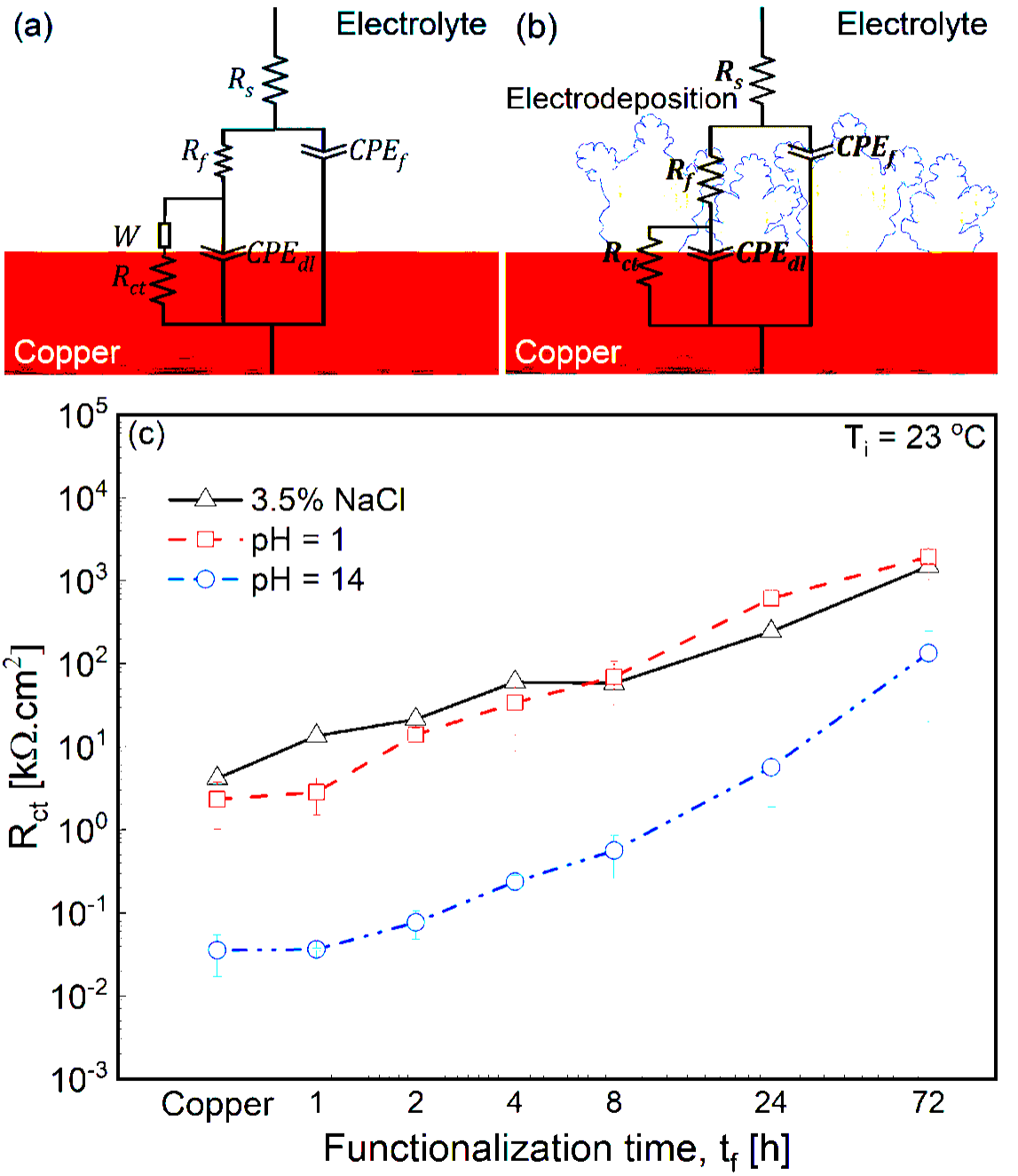

Figure 6: Mousavi and Pitchumani

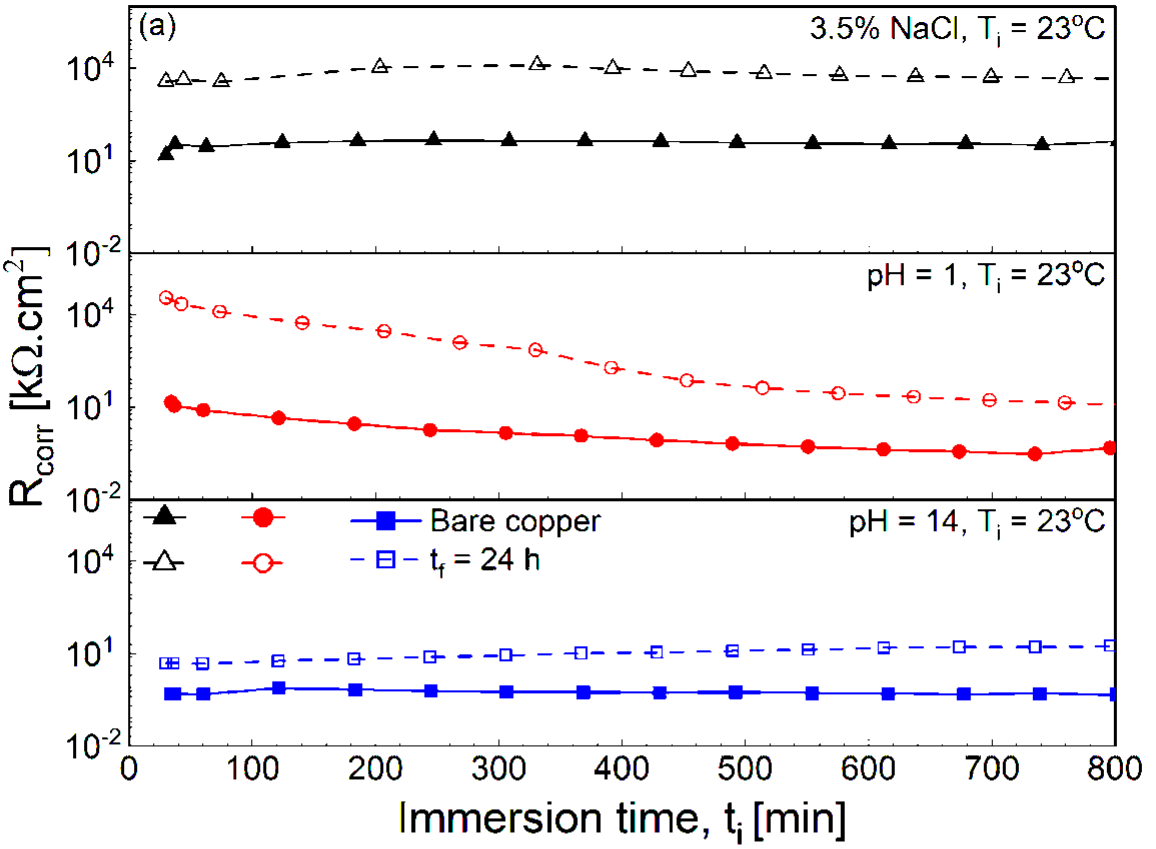

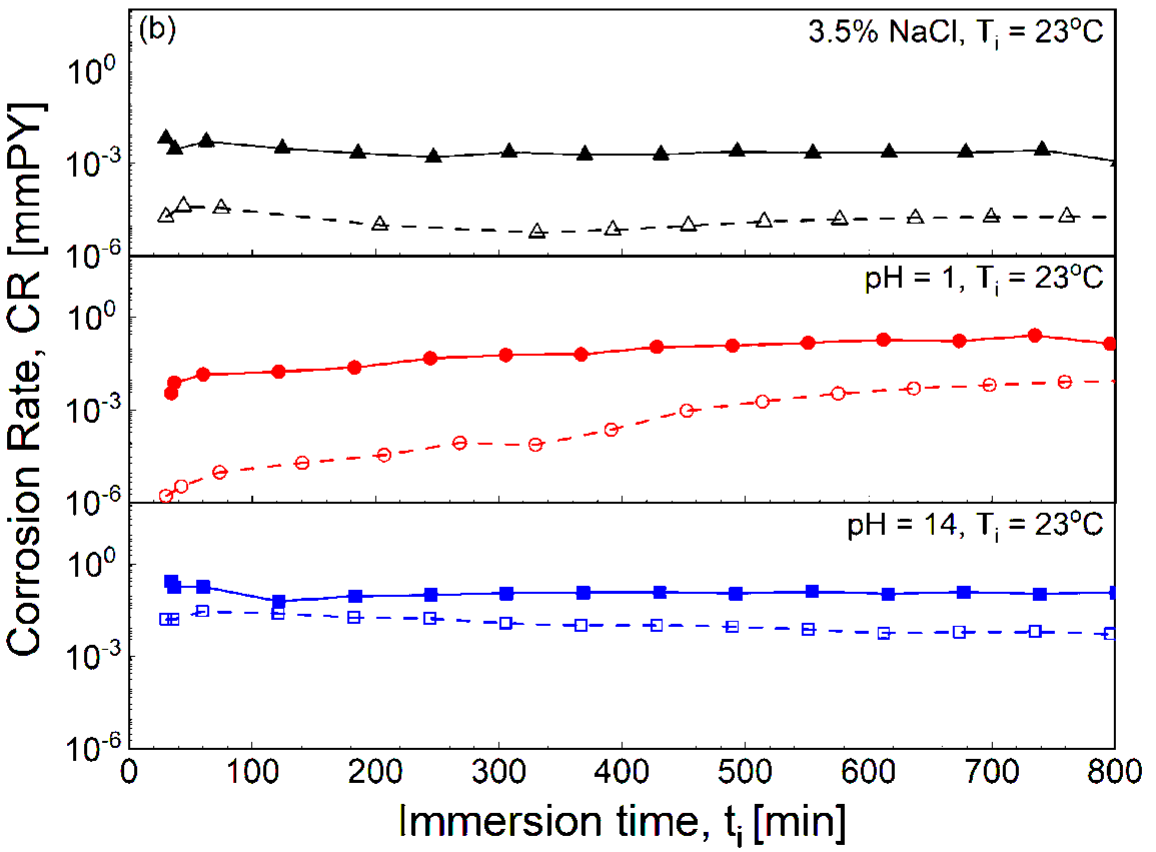

Figure 7: Mousavi and Pitchumani

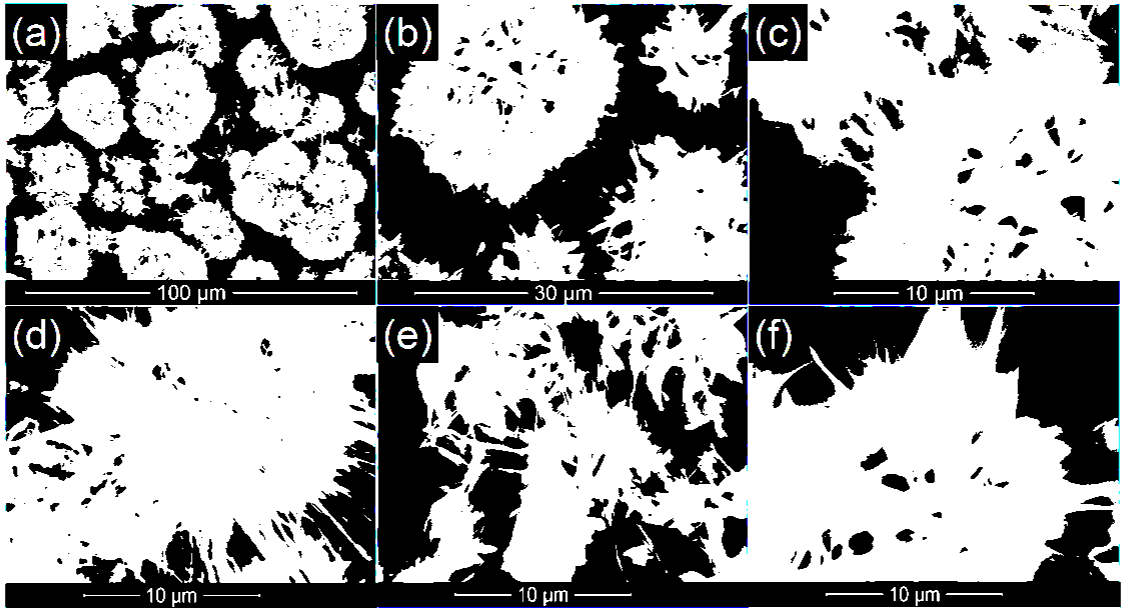

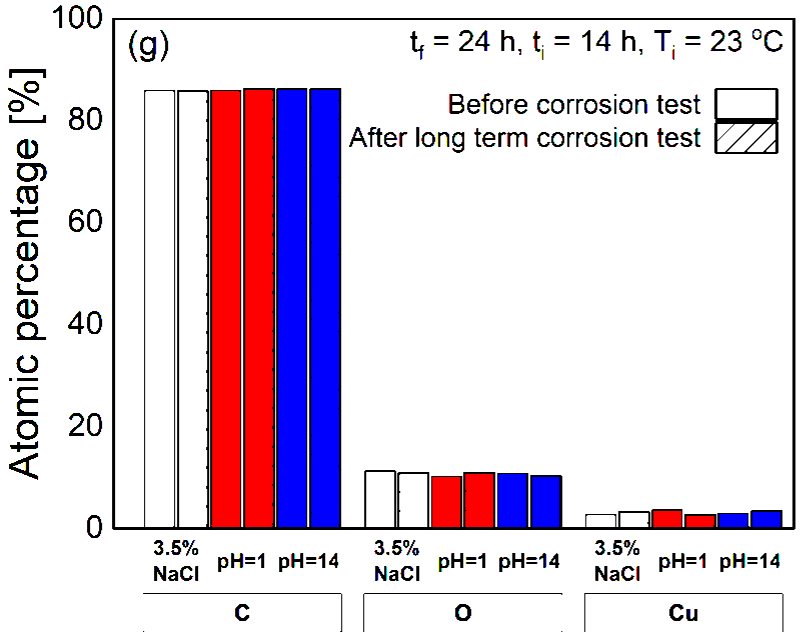

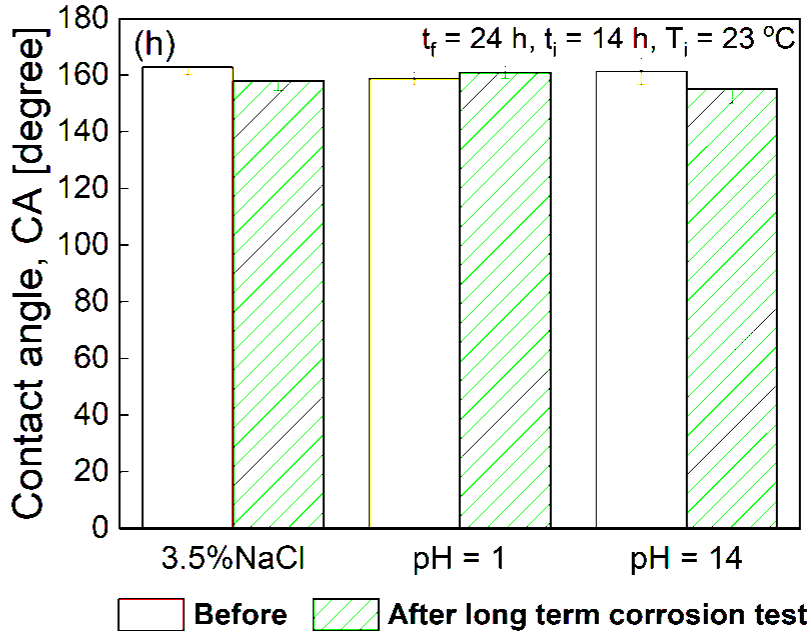

Figure 8: Mousavi and Pitchumani

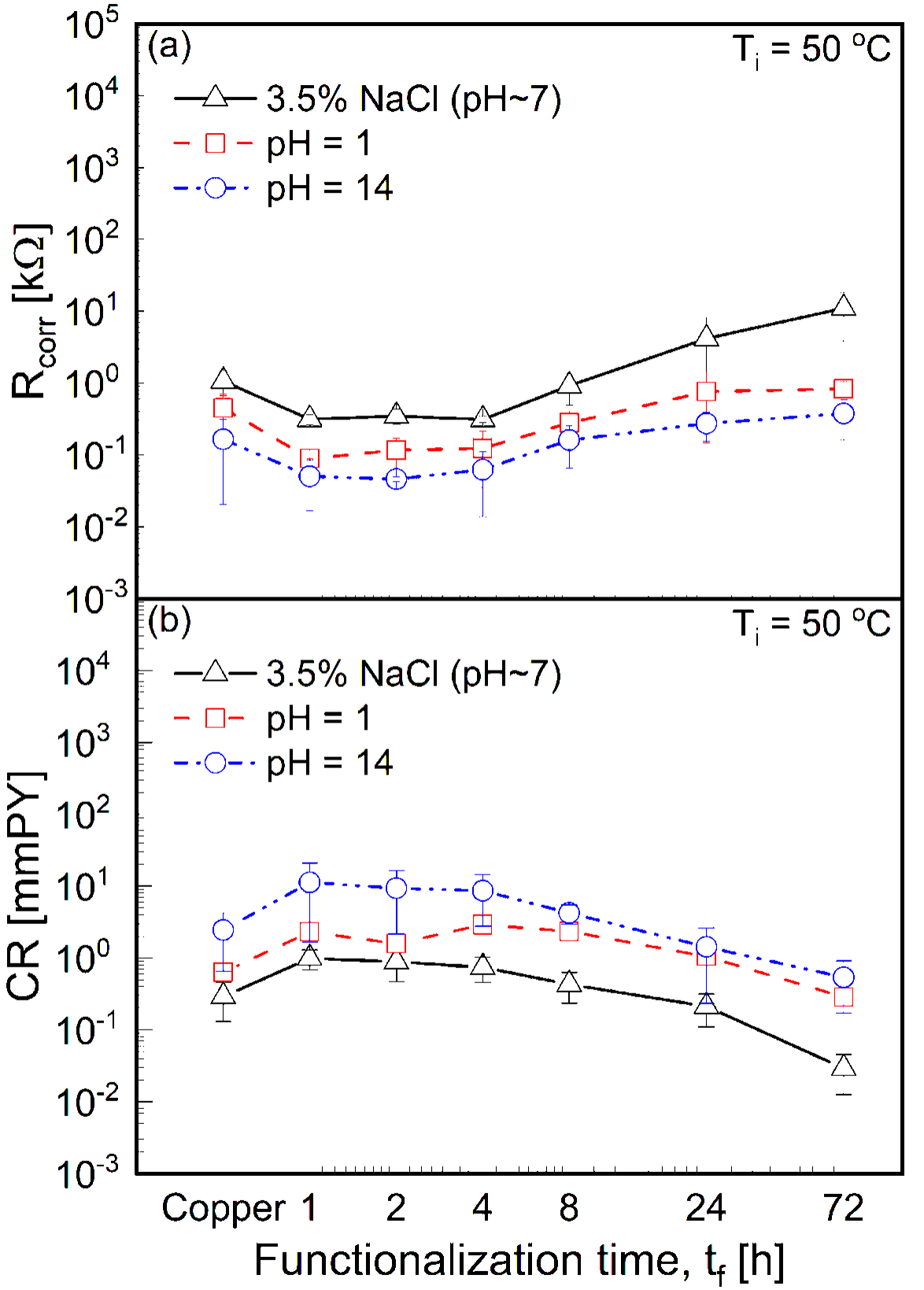

Figure 9: Mousavi and Pitchumani

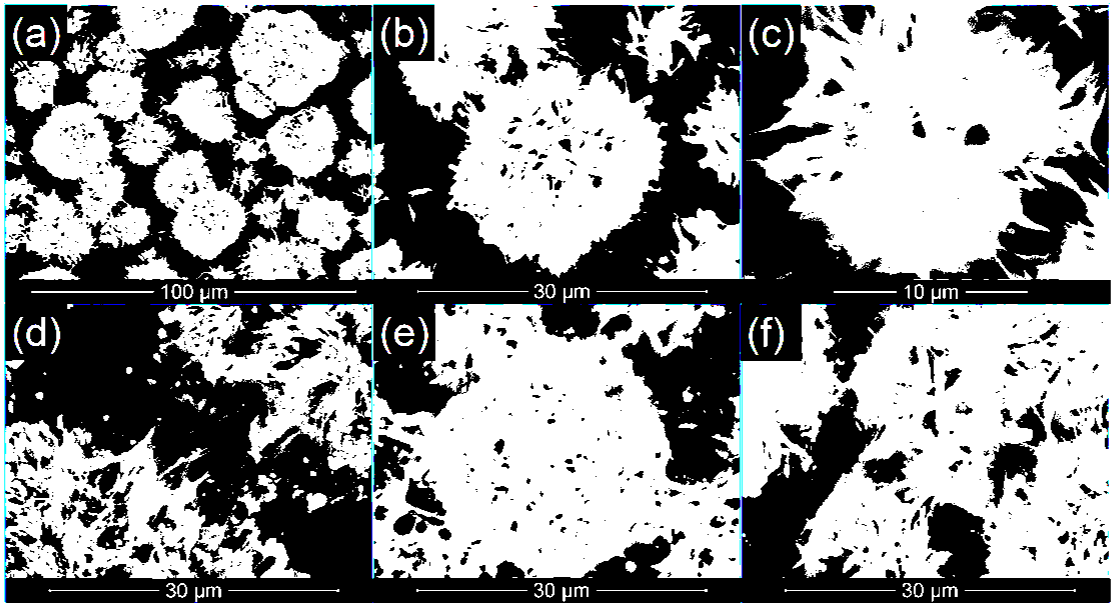

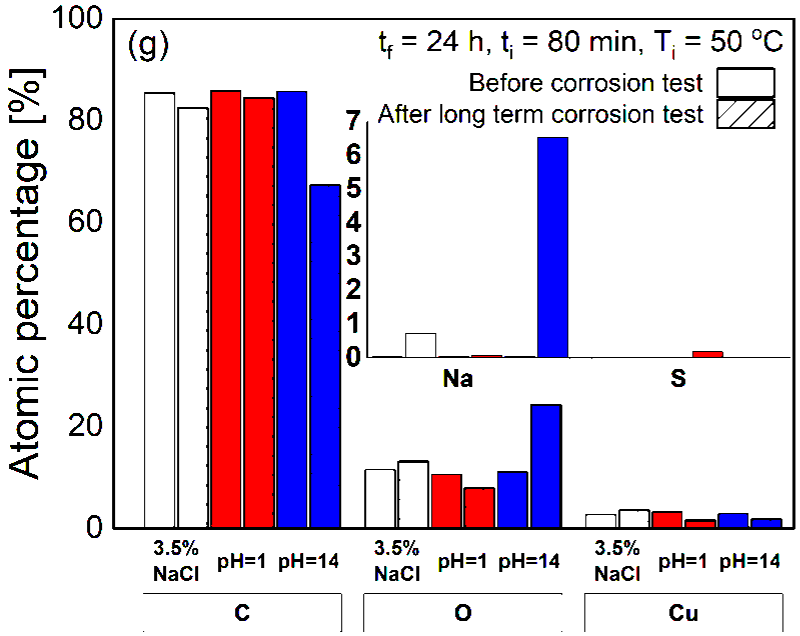

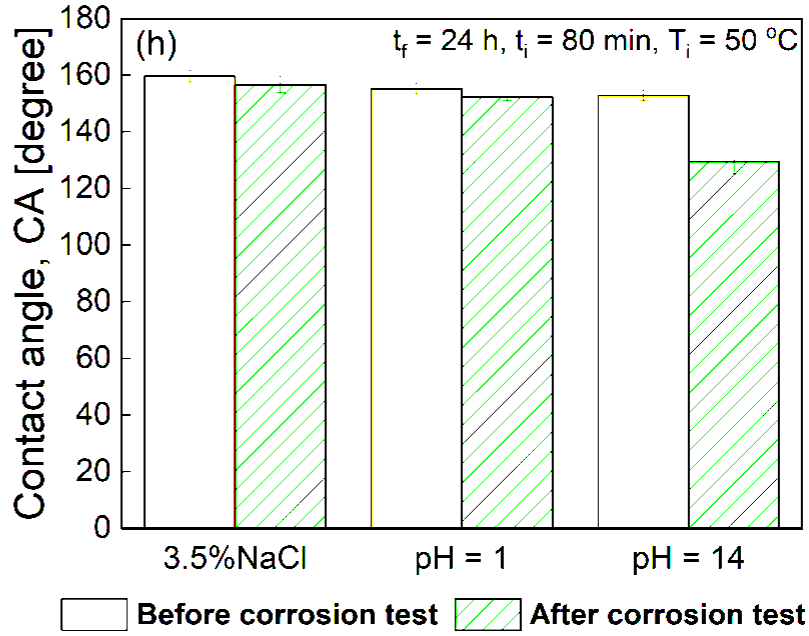

Figure 10: Mousavi and Pitchumani

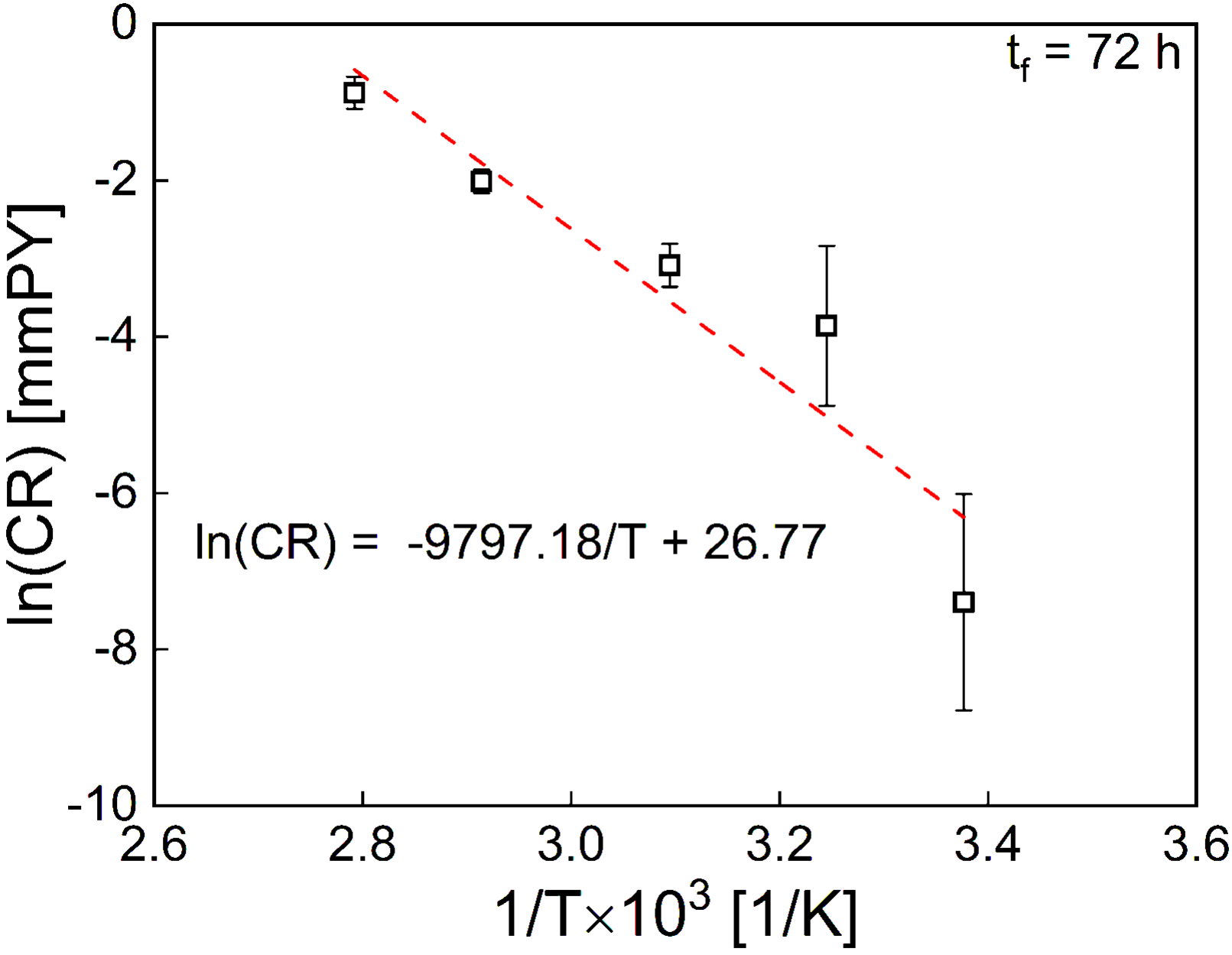

Figure 11: Mousavi and Pitchumani

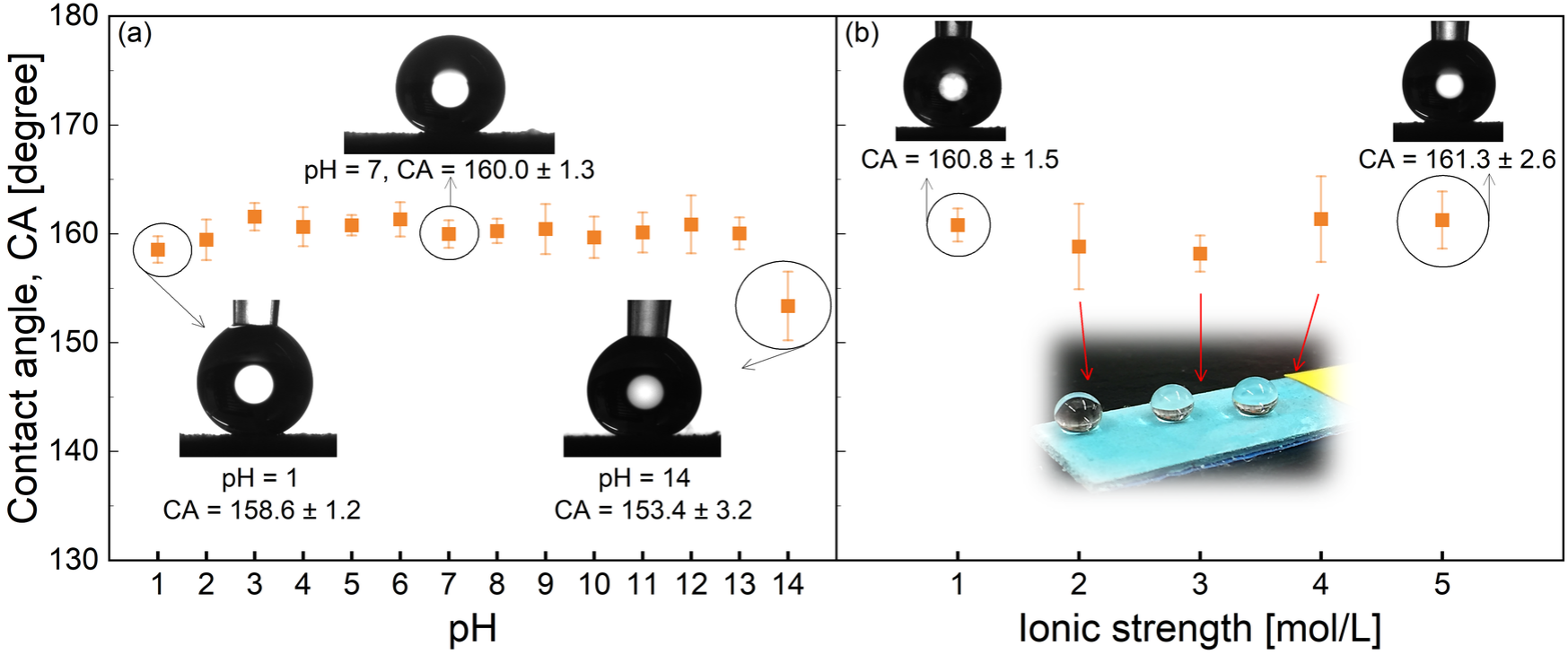

Figure 12: Mousavi and Pitchumani